University of Cincinnati

Date: 4/16/2012

I, Nithin S Panicker , hereby submit this original work as part of the requirements for the degree of Master of Science in Mechanical Engineering.

It is entitled:

Numerical Modeling of Flow and Deformations Induced in a Droplet Subjected to Alternating Electric Field

Student's name: **Nithin S Panicker**

This work and its defense approved by:

Committee chair: Milind Jog, PhD

Committee member: Shaaban Abdallah, PhD

Committee member: Raj Manglik, PhD

2569

Numerical Modeling of Flow and Deformations Induced in a Droplet Subjected to Alternating Electric Field

A Thesis submitted to the

Graduate School

of the University of Cincinnati

in partial fulfillment of the

requirements for the degree of

MASTER OF SCIENCE

In Mechanical Engineering

2012

By

Nithin S Panicker

Committee Chair: Dr. Milind Jog

ABSTRACT

Numerical investigation of the flow in a drop of a dielectric fluid suspended in another immiscible dielectric fluid in the presence of an alternating electric field has been carried out. When an electric field is applied to a drop of a dielectric fluid, the electric field induces stresses at the fluid interface. The normal stresses deform the drop and the tangential stresses produce a circulatory motion inside and outside the drop. Such electrical field induced flow can lead to significant enhancement of heat or mass transfer to from the drop. A stream function-vorticity approach with a finite volume formulation is adopted to numerically determine the unsteady flow field in the continuous and the dispersed phases. The volume of fluid (VOF) method is used to track the phase boundary and to predict the transient drop shape deformations for a range of capillary numbers. A new VOF formulation with Continuum Surface Force model has been derived and implemented to account for both the tangential and the normal electrical stresses present at the phase interface. Results show that the extent of drop deformation increases with capillary number and the strength of the electric field. By tracking Lagrangian fluid particles inside the deforming droplet, it is seen that the changing flow patterns due to drop deformation lead to significant fluid mixing inside the droplet. Earlier studies available in the literature neglect drop deformations and may significantly underestimate the heat/mass transfer enhancement in the presence of an alternating electric field.

ACKNOWLEDGEMENT

I gratefully acknowledge my advisor, Dr. Milind Jog for the guidance, support and continual encouragement during the course of study and research work; the committee members Dr. Raj Manglik and Dr. Shabaan Abdallah for their support. I would also like to thank my parents, sister and friends for their love and moral support.

Contents:

LIST OF FIGURES:

LIST OF TABLES:

NOMENCLATURE:

r	Dimensionless radius [m]
t	Time [s]
p	Pressure [N/m^2]
R	Length of the domain [m]
a	Radius of the drop [m]
U	Maximum velocity [m/s]
f	Volume fraction
E	Electric field [V/m]
Ca	Capillary number
Ce	Electric capillary number
V	Voltage [V]
k_ν	kinematic Viscosity ratio [m^2/s]
Re	Reynolds number
k_ρ	Density ratio
k_{di}	Dielectric constant ratio
k_σ	Conductivity ratio
u_r	Velocity in the r-direction [m/s]
u_θ	Velocity in theta-direction [m/s]

k	Dielectric constant

Greek

Symbols:

μ	Dynamic viscosity [Pa-s]
ρ	Density [kg/m^3]
ψ	Stream function [m^2/s]
ω	Vorticity [s^{-1}]
κ	Curvature [m^{-1}]
γ	Surface tension coefficient [N/m]
σ	Conductivity [Ω m^{-1}]

Superscripts:

*	Dimensional quantities

Subscripts

1	Continuous phase(medium)

2	Dispersed phase(Drop)

CHAPTER 1

INTRODUCTION

1.1 Motivation and Significance:

To develop energy efficient heat and mass transfer processes, augmentation of heat/mass transfer by application of electric field is being explored in two-phase systems. Examples include heat transfer in direct-contact compact heat exchangers and mass transfer in chemical extraction where droplets of one liquid move through another liquid. When an electric field is applied on a dielectric drop, a charge build up occurs at the drop/continuous phase interface which induces stresses both in tangential and normal direction. The tangential stresses induce fluid motion in the neighborhood of the interface and normal stresses causes drop deformation. This electrically induced motion can be used to enhance the heat/mass transfer. For example, for a drop of a liquid that is being heated, the electrically induced flow will bring hot fluid towards the drop and bring cold fluid from drop interior to the drop surface and significantly increase heat transfer compared to conduction.

It has been shown that the maximum increase in the rate of heat transfer with uniform DC electric field is 67% compared to heat transfer to a purely translating drop without application of electric field (Oliver et al. 1985) for a spherical drop. However, only under certain combination of electrical and thermo-physical properties of the two fluids, the drop can remain spherical (Taylor, 1966). In most cases, the drop will either deform as a prolate or an oblate spheroid. The enhancement in heat/mass transfer is higher in deformed drop compared to a spherical drop (Hader & Jog, 1998, Jog & Hader, 1997). Recent studies have shown that with the application of an alternating electric field, significant fluid mixing inside the drop can be induced (Bryden & Brenner, 1998, Ward & Homsy, 2001, Ward and Homsy 2003, Christov & Homsy, 2009, Abdelaal & Jog, 2011, and Abdelaal & Jog, 2012). For a DC electric field, the drop deforms during initial transients and the deformation remains constant thereafter. However, for a time-modulated electric field, the drop deformation as well as flow inside the drop is expected to change with time in a periodic fashion. It is hypothesized that alternating electric field will cause a time varying flow field and continuous drop oscillations that will lead to better mixing inside the droplet. Improvements in fluid mixing inside the drop correspond to significantly higher heat transfer rates. The aim of the work is to computationally model the complex two-phase flow field and interface deformation under the influence of alternating electric field and to determine the effect of drop deformation on fluid mixing inside the drop.

The complex fluid flow behavior inside and outside the drop due to the combined effect of tangential and normal stresses coupled with the shape change due to oscillation of the drop makes the study a challenging task. Recent advances in numerical methods to model the continuously deforming two-phase interface will be used, to accurately determine the droplet shape change, internal and external flow parameters will be quantified for different electric field strength. The results will provide fundamental insights into deforming multiphase interfaces and concomitant heat/mass transfer, and will be useful to practicing engineers to design direct contact heat exchangers and mass transfer devices.

1.2 Scope:

Flow and shape deformations are numerically modeled for a droplet of a dielectric fluid suspended in another immiscible fluid subjected to an alternating electric field. The Volume-of-Fluid (VOF) method is used to track the two phase interface and determine the instantaneous drop shape. Because the VOF method spreads the interface over two or three grid cells, a new method was developed to incorporate the interfacial tangential stress induced by the electric field. The electric field in the two phases is determined at each time step and the corresponding interfacial stresses are evaluated. The drop shape and the electric field-induced flow inside the drop are obtained by solving the Navier-Stokes equations in the two phases. A stream-function-vorticity formulation is adopted for this purpose. Using the developed numerical model, drop behavior is simulated for different capillary numbers. When capillary number is very small, a Lagrangian particle inside the drop follow closed streamlines. However, as the capillary number increases, the particle paths tend to cover a larger domain indicating enhanced fluid mixing.

A review of the pertinent literature is presented in chapter 2. Mathematical formulation of the problem including the governing equations for flow and electric field along with the appropriate boundary conditions are outlined in chapter 3. A new method to incorporate interfacial stresses in the VOF framework is derived in chapter 4. Results are presented and discussed in chapter 5. A summary of the finding of this study and recommendations for future work are listed in chapter 6.

CHAPTER 2

LITERATURE SURVEY

2.1 .Drop deformation:

Chester et al. (1953) were perhaps the first to report deformations in a dielectric drop suspended in a dielectric medium subjected to a uniform electric field. They considered a drop of volume $4/3\,\pi\,r^3$, of a material of inductive capacity e_2, suspended in a medium e_1, to which was applied a parallel electric field of strength E. The distortion of the drop was assumed to be very small so that the shape of the droplet may be approximated as an ellipsoid of minor axis and major axis b with an eccentricity e. They derived an analytical expression for eccentricity e in terms of the Electric strength E by minimizing the surface energy of the droplet. They found from the expression that irrespective of the polarity of the electric strength, the droplet always elongated in the direction of the field whether its dielectric constant is greater or less than that of the surrounding medium for the case where the surrounding medium can be regarded as perfect dielectric.

Allan & Mason (1962) found that, on the exposure of drop of a dielectric fluid which is suspended in another dielectric fluid to a steady electric field leads to local charge accumulation on the interface causing tangential electrical stresses. These tangential stresses, induce circulation of the fluid inside and outside the drop. This was first demonstrated by (Taylor, 1966) in his experiments with silicone oil drops suspended in a mixture of castor oil and corn oil as shown in Figure 1. The normal stresses cause the droplet to deform.

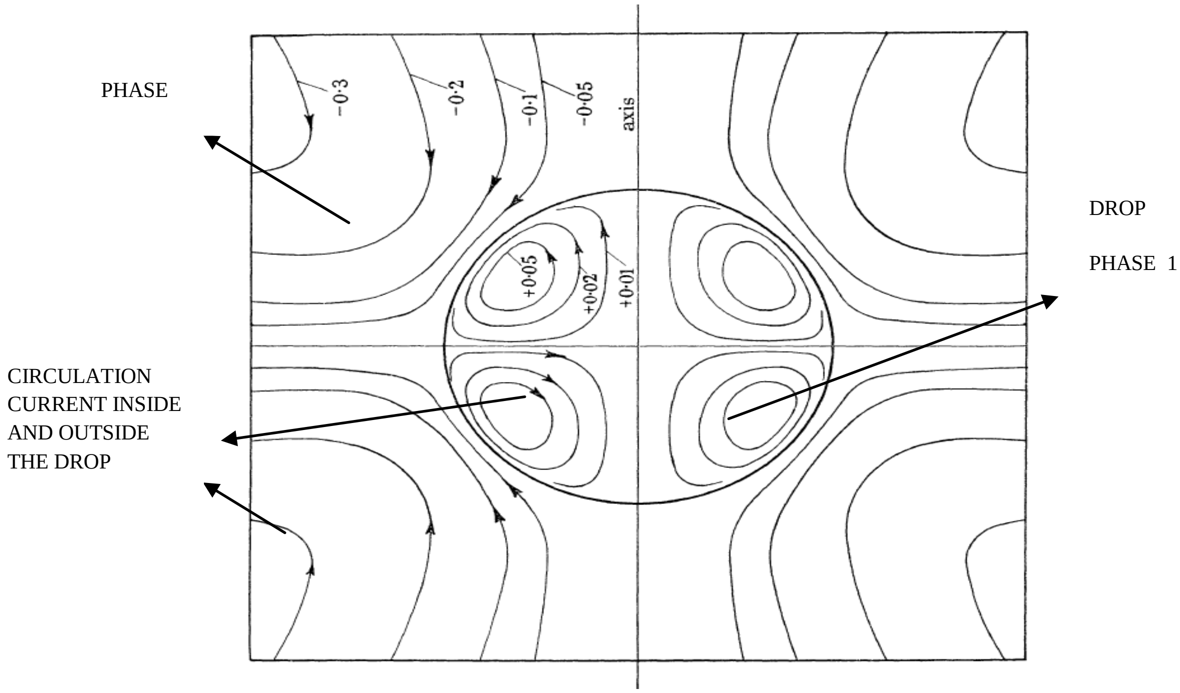

Figure.1. Circulation inside the droplet due to electric field

Torza, Cox & Mason (1971) did both experimental and analytical study on the deformations in a droplet suspended in a dielectric medium when subjected to an alternating electric field for different frequencies from υ= 0 Hz to υ = 60 Hz and thermo physical properties both. According to their experimental study, the spherical droplet always deformed into a prolate spheroid at υ = 60 Hz for at least 22 drop/medium combinations. This suggested that in systems which formed oblate spheroids at υ = 0 Hz there should exist a critical frequency υc at which no deformation occurs no matter how high the field. They also observed that at υ = 1 Hz the drop oscillated twice as fast as the field with a significant oscillation of the drop surface. A number of other differences in modes of deformation between υ = 0 Hz to υ = 60 Hz were observed which couldn't be explained by Taylor's theory which, strictly speaking applies only at $\upsilon = 0$ Hz.

The drop circulation and deformation caused due to electric field can significantly influence the mass and heat transport inside a droplet leading to an enhancement in these transports.

2.2. Enhancement in mixing in a drop subjected to electric field

Oliver et al. (1985) numerically investigated the transient heat transfer to a neutrally buoyant droplet suspended in an electric field and compared it with a translating drop in the absence of electric field. Although the deformations due to normal stresses were not considered in their study, they have found a significant enhancement in mixing of 67% higher than the translating drop.

Subramanian & Jog (2005) studied the enhancement of heat transfer by electric field in a translating drop. Their study unlike (Oliver et al., 1985) involved both translational and electrical effect on the flow field, but with no deformation. They found that the enhancement in heat transfer caused due to both translational and electric field driven flow is substantially greater than that of purely translational flow or purely electrically driven flow.

Hader & Jog (1992) studied the effect of droplet deformation due to steady electric field on enhancement in heat transfer .An electrically induced flow field was determined for both prolate and oblate drop shapes. They concluded that enhancement in heat transfer for oblate drops are significantly higher than those for prolate drops, hence the enhancement of direct contact heat or mass transfer is more effective for a combination of liquids for the continuous phase and the drop phase that leads to an oblate deformation of the drop under the application of an electric field.

Christov & Homsy (2009) studied the transport of heat or mass from circulating droplets that are both settling and subject to an axial unsteady electric field with no deformations, as a function of four dimensionless numbers Peclet number Pe, the dimensionless amplitudes of both the steady and unsteady electric field and the dimensionless frequency(ω) of the modulation. There results suggest that for a steady drop the enhancement factor is higher with Taylor flow than without. For modulated electric field the enhancement factor is not a simple function of parameters and shows resonant peaks at particular values of (ω) for which the enhancement factor is extremely large.

Meizhong et al. (2002) studied the effect of droplet oscillation on internal heat transfer numerically using a three dimensional Navier Stokes solver for free surface flows. The oscillation was induced by perturbing the droplet initially and allowing it to stabilize. There hypothesis on enhancement in heat transfer was supported by their results but the effect of the magnitude Nusselt number was very small. They also concluded that a continuous perturbation of the droplet with a constant source have a higher chance in improving mixing.

The above literature review shows that application of electric field to enhance heat or mass transfer from liquid drops has received much attention in the literature. Both steady and alternating fields have been considered but all of the work deals with steady electric field with no deformation, unsteady electric field with no deformation and deformation with no electric field due to complexities involved in modeling changing flow field, drop shape changes and integration of electric field with changing drop shape. The current study is based on coupling both drop deformation and unsteady (alternating) electric field, and its effects on heat and mass transport inside a neutrally buoyant drop.

2.3. Numerical methodology to capture drop dynamics:

The two phase flow involving droplet and the medium it is suspended poses a challenging task to accurately determine the interface of these two phases. The numerical method developed to capture the free interface should have the following features:

1. A scheme to compute the shape and locate the interface accurately,
2. Evolution of the shape and location with time accurately.
3. Effect of the change in shape on both the droplet and the medium.

Many numerical methods have been developed in the recent past to track the interface and these methods are used widely in the study of physical phenomena such as bubbles, wind-water-wave-extraction etc. Some commonly used methods for interfacial tracking for two-phase flows include Lagrangian grid methods, Marker particle method front-tracking, level-set and the volume-of-fluid (VOF) method. These methods are outlined below:

2.3.1. Lagrangian grid methods

The interface can be tracked by a Lagrangian grid which moves with the fluid. The grid movement linked with the fluid movement results in tracking of the interface. Examples can be found in (Hirt & Nichols, 1979). However, as the interface evolves the grid used in Lagrangian methods will change at each time step, since the values at the new grid points need to be approximated from the old grid, errors are induced. Furthermore, the Lagrangian grid method cannot track the interface when the amplitude is large, and it cannot handle a breaking interface.

2.3.2. Marker and cell method (MAC)

The MAC method is one of the earliest numerical methods used to track the interface evolution in fixed Eulerian grid. It was first introduced by (Harlow & Welch, 1965). The location of the fluid within a grid cell is tracked by a set of markers that move along with the fluid. The free interface is considered passing through a grid cell if that cell has at least one neighboring grid cell which is empty (with no markers in it). Evolution of the free interface is calculated by moving the markers along the fluid flow. The MAC method doesn't track the interface directly, instead it tracks the evolution of the fluid volume. The interface is then the boundary of the fluid. Many improvements have been added to the original MAC method to improve accuracy or include other physical aspects, such as surface tension on the interface. However one of the limitations for the MAC method is that in order to achieve a certain accuracy, it requires high computational costs associated with the required number of markers, especially when the deformation of the interface is large.

2.3.3. Volume of fluid (VOF)

The VOF method (Hirt & Nichols, 1981) was first introduced to maintain similar features of the MAC method, but with reduced computational cost. In the VOF method, only one fluid quantity, the fluid volume fraction, is used. The fluid volume fraction (say, F) is defined as a function which gives the percentage of phase 1 in a grid cell. Hence, F = 0 for the grid cell in the phase 2 and F = 1 for the grid cell in the phase 1. Function F will only achieve some values between 0 and 1 if the grid cell is at the interface. The slope and the curvature of the interface is calculated using the volume fractions in the neighboring cells and the interface location is determined by the slope, curvature, as well as the volume fraction.

To compute the time evolution of the interface, the basic kinematic equation for the fluid volume fraction is used which for an incompressible flow,

$$\frac{Df}{Dt} = 0 \tag{1}$$

$$\frac{\partial f}{\partial t} + \left(\vec{u}.\nabla\right) f = 0 \tag{2}$$

Where the velocities are updated using the Navier-Stokes Equations. The VOF method has been used widely and has been applied successfully in much different applications. VOF method complies with mass conservation. Consider a grid cell (i, j) with volume fraction f then the volume of phase 1 in that cell at a particular time n will be $f_{i,j}^{n}$ V, where V is the volume of the cell. A natural definition of mass conservation for an incompressible flow is a method which conserves the total volume at each time step so that

$$\sum_{ij} f_{i,j}^{n} = \sum_{ij} f_{i,j}^{n+1} \tag{3}$$

Eqn. (1) perfectly realize the condition given in Eqn. (3) which proves the method complies with mass conservation unlike other methods. However, the VOF method has trouble capturing the exact location of the interface, exact location of the interface is required to apply the interfacial forces like surface tension. This can be overcome by interface reconstruction (Aulisa et al., 2007) but with high computational cost. In the current study, CSF (Continuum surface force model) method is used to provide the interfacial forces, which eliminates the need of interface reconstruction and reduces the computational cost.

2.3.4. Level set method

Level set method (Osher & Sethian, 1988) unlike the MAC method tracks the shape rather than the particle itself. These methods are advantageous over the particle tracking methods in problems involving splitting of the curve, developing holes etc. The greatest advantage of Level set methods are the numerical computation of tracking the interface can be performed in a single grid without having to use a moving grid. The main disadvantage of Level set method is that it doesn't ensure mass conservation unlike the VOF method discussed above. There are conservative level set methods like CLSVOF (Sussman & Puckett, 2000) which is difficult to implement computationally hence not used in the current work.

2.3.5. Continuum surface force model (CSF)

The continuum surface force model (CSF) (Brackbill et al., 1992) is a method to model the forces at the interface namely surface tension force, electrical force etc. The forces at the interface like surface tension forces are surface forces, which often become a boundary condition for most of the two phase flow problems.

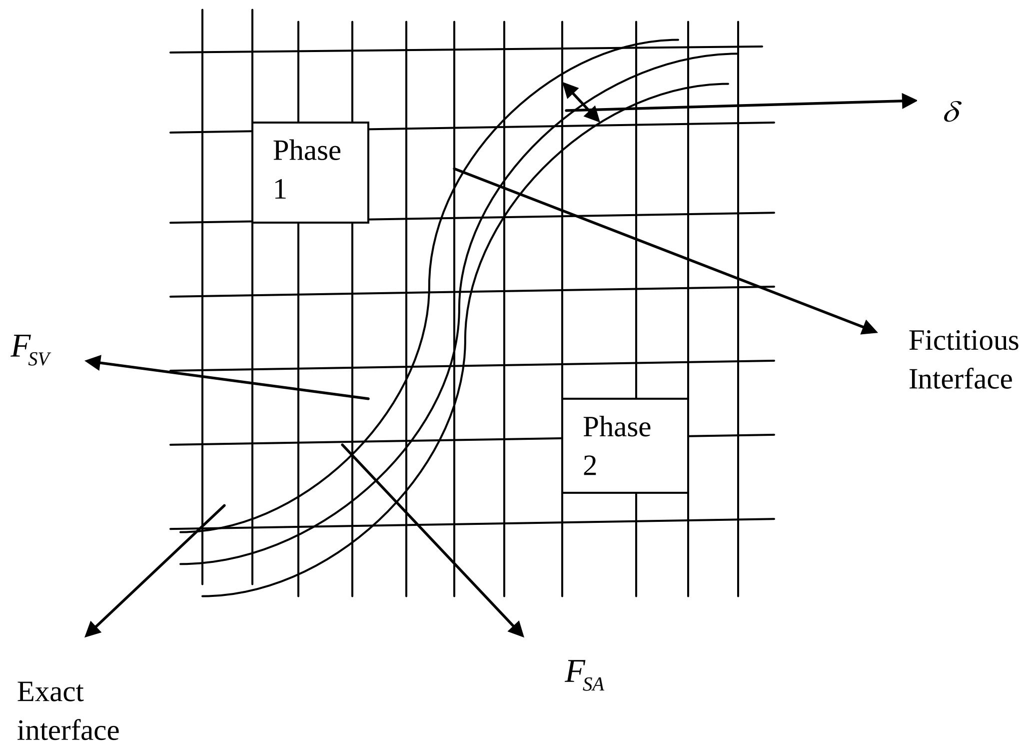

Figure 2. Interface band

Accurate location of an interface in a two phase flow is a numerically challenging task, existing methods in the literature like PLIC (piecewise linear interface calculation), SLIC (simple line interface calculation) (Noh et al., 1976), are difficult to implement and computationally expensive.

CSF model eliminates the need of an exact location of the interface thereby simplifying the calculation. It considers the interface as a band of width δ where, $\delta \to 0$ as shown in Fig. 2. The forces acting at the interface which was a single surface of surface area A is converted in to a force which acts inside a band of volume V such that the net force acting on a surface is same as the force acting on the volume as shown in Eqn. (1).

$$\int_A \overrightarrow{F_{SA}} d\vec{A} = \lim_{\delta \to 0} \int_V \overrightarrow{F_{SV}} dV \tag{4}$$

The above equation is only satisfied when,

$$\overrightarrow{F_{SV}} = |\overrightarrow{F_{SA}}| \frac{\nabla \tilde{c}(\vec{x})}{[c]} \tag{5}$$

The VOF method works very effectively with CSF approach because the later assumes interface to be a band in which the volume fraction varies from 0 to 1.

2.4. Characterization of mixing:-

Bryden & Brenner (1998) investigated the mixing properties of a droplet translating by buoyancy through an immiscible liquid which is undergoing simple shear by qualitative measures of the extent of mixing, accompanied by visualization of the regions exhibiting high mixing in the form of Poincare sections by Lagrangian particle tracking approach. This study made by Bryden and Brenner being the key motivation to study the mixing in the current work by Lagrangian particle tracking method.

2.4.1. Lagrangian particle tracking (lpt):-

Lagrangian particle tracking is used to determine the trajectory of a particle immersed within the currents of a fluid. LPT gives a visual indication of scalar transport in a system. In the current study LPT is used to qualitatively determine the mixing induced in a droplet due to droplet oscillations. It gives the transient streamlines inside a droplet while it is oscillating.

The equation governing the Lagrangian trajectories of a fluid particle $\vec{x} = \vec{x}(\vec{x}_o, t)$ inside an oscillating droplet, with $\vec{u}$ the velocity vector due to the flow field inside is:

$$\frac{d\vec{x}}{dt} = \vec{u} \tag{6}$$

Where $\vec{x}$ is the position vector of the particle and $\vec{x}_o$ is the initial position of the particle. Multiple particles are tracked in the current study to get an elaborate picture of mixing taking place inside a droplet.

CHAPTER 3

FORMULATION

3.1. Problem description:

We consider a spherical fluid drop as shown in Fig. 3 of radius R, density ρ_2, viscosity μ_2, dielectric constant k_2, electrical conductivity σ_2, suspended in a fluid of density ρ_1, viscosity μ_1, dielectric constant k_1, electrical conductivity σ_1. The interface separating the two fluids is assumed to have a constant surface tension coefficient γ so that the variation in surface tension force along the tangential direction can be neglected. An alternating voltage $V = V_0 \sin \omega t$ is applied using the parallel plates to generate an alternating and uniform electric field E along the z-direction. The electric field generated induces stresses at the drop interface and deforms the drop depending on the properties. To study the two phase system effectively the properties are defined in terms of property ratios: $k_\rho = \rho_1/\rho_2$, $k_\nu = \nu_1/\nu_2$, $k_{di} = k_1/k_2$, $k_\sigma = \sigma_1/\sigma_2$. The density ratio k_ρ = 1 so that the drop is neutrally buoyant and viscosity ratio k_ν is kept close to 1 to avoid numerical instability due to large gradient in properties and study can be centered only on the effects of electrical forces and surface tension forces on the deformation.

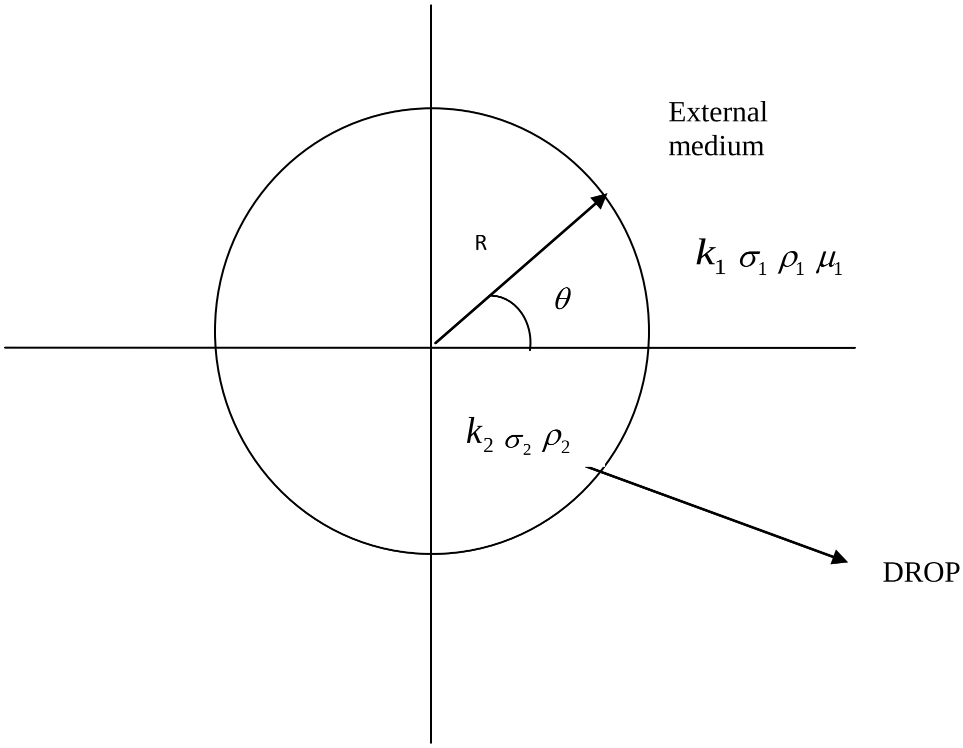

Figure.3. A schematic of the droplet and the coordinate system

3.2. Coordinate system:

The flow and the volume fraction transport equations are solved on a spherical coordinate system Fig. 3 for the dispersed phase (phase 2) or the drop phase. A transformed domain with a transformation of $r = e^z$ along the *r*-direction is used to solve the equations in continuous phase (phase 1) or the phase which contains the medium. The grid is shown in Fig. 4. The transformation is performed so that the grid is finer near the interface, which is domain of interest, and the grid becomes coarser as we proceed from the interface to the computational infinity where all gradients are expected to be very small. The computational infinity is chosen to be r = 148 or z = 5 such that the boundary effect is negligible (Subramanian, 2005).

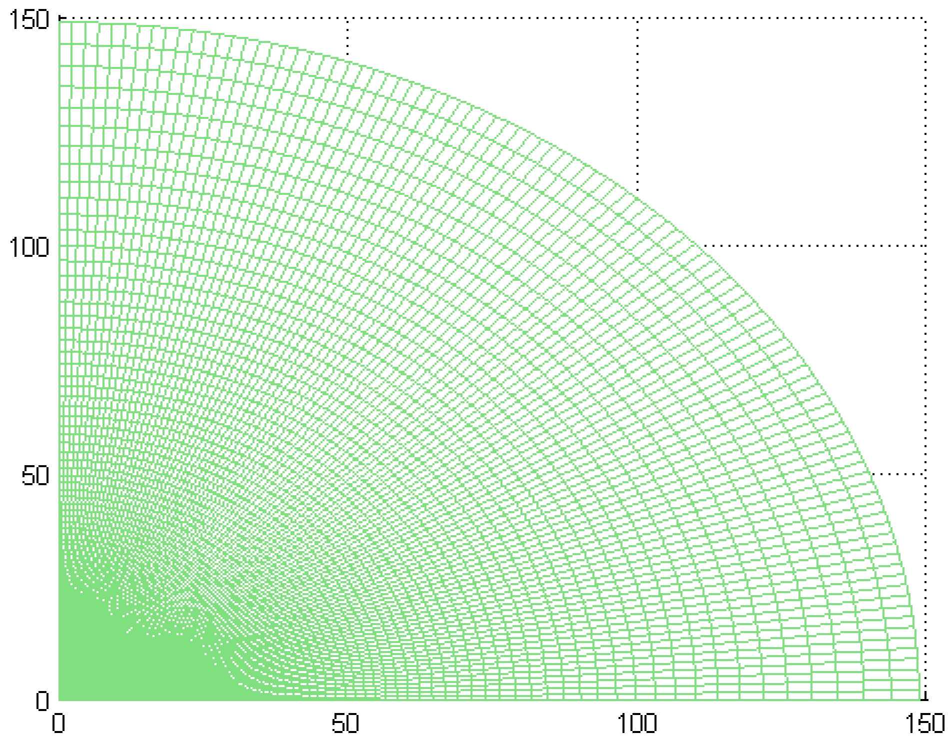

Figure. 4. Grid

3.3. Mass conservation equations:-

For a steady incompressible flow the mass conservation equation is:

$$\nabla^{*}.\overrightarrow{u^{*}} = 0 \qquad (7)$$

By non-dimensionalizing the above equation by the following factors

$$u = \frac{u^{*}}{U} \qquad \nabla = a\nabla^{*}$$

We get :

$$\nabla.\vec{u} = 0 \tag{8}$$

3.4. Momentum conservation equations:-

For an unsteady incompressible two-phase flow the governing equations in vector form are:-

$$\frac{\partial\left(\rho\overrightarrow{u^*}\right)}{\partial t} + \rho\overrightarrow{u^*}.\nabla^*\overrightarrow{u^*} = -\nabla^* p^* + \mu\nabla^{*2}\overrightarrow{u^*} + \vec{F} \tag{9}$$

where,

$$\mu = \mu_2 f + (1-f)\mu_1 \qquad \rho = \rho_2 f + (1-f)\rho_1$$

The above equation is non-dimensionalized by the following factors:

$$u = \frac{u^*}{U} \quad p = \frac{p^*}{\mu_{ref}U/a^2} \quad \nabla = a\nabla^* \quad F = \frac{F^*}{\mu_{ref}U/a^2} \quad t = \frac{t^*}{a^2\rho_{ref}/\mu_{ref}}$$

μ_{ref} **,** ρ_{ref} **-** reference viscosity and density are taken to be that of fluid 2 (fluid inside the droplet)

The non-dimensionalized form of the equation is:

$$\frac{\partial\left(\rho\vec{u}\right)}{\partial t}+\rho\vec{u}.\nabla\vec{u}=-\nabla p+\mu\nabla^{2}\vec{u}+\vec{F} \tag{10}$$

$$\frac{1}{\mathrm{Re}}\frac{\partial\vec{u}}{\partial t}+\vec{u}.\nabla\vec{u}=-\frac{1}{\mathrm{Re}\,k_{\rho}}\nabla p+\frac{1}{\mathrm{Re}}k_{\nu}\nabla^{2}\vec{u}+\frac{1}{\mathrm{Re}\,k_{\rho}}\vec{F} \tag{11}$$

By multiplying both sides by **Re** we get:

$$\frac{1}{\mathrm{Re}}\frac{\partial\vec{u}}{\partial t}+\vec{u}.\nabla\vec{u}=-\frac{1}{\mathrm{Re}\,k_{\rho}}\nabla p+\frac{1}{\mathrm{Re}}k_{\nu}\nabla^{2}\vec{u}+\frac{1}{\mathrm{Re}\,k_{\rho}}\vec{F} \tag{12}$$

$$\frac{\partial\vec{u}}{\partial t}+\mathrm{Re}\vec{u}.\nabla\vec{u}=-\frac{1}{k_{\rho}}\nabla p+k_{\nu}\nabla^{2}\vec{u}+\frac{1}{k_{\rho}}\vec{F} \tag{13}$$

Since we are dealing with low Reynolds number (Re $\rightarrow$ 0) flow, the inertia term $\mathrm{Re}\vec{u}.\nabla\vec{u}$ will be small compared to the other terms and it be neglected so that the equation becomes:

$$\frac{\partial\vec{u}}{\partial t}=-\frac{1}{k_{\rho}}\nabla p+k_{\nu}\nabla^{2}\vec{u}+\frac{1}{k_{\rho}}\vec{F} \tag{14}$$

3.4.1. Stream function-vorticity formulation of momentum equation:-

Vorticity $\vec{\omega}$ can be defined as

$$\vec{\omega}=\nabla\times\vec{u} \tag{15}$$

By taking a curl of Eqn. (6) we get

$$\frac{\partial\left(\nabla\times\vec{u}\right)}{\partial t} = k_\nu \nabla^2\left(\nabla\times\vec{u}\right) + \frac{1}{k_\rho}\nabla\times\vec{F} \tag{16}$$

$$\frac{\partial\vec{\omega}}{\partial t} = k_\nu \nabla^2\vec{\omega} + \frac{1}{k_\rho}\left[\frac{1}{r}\frac{\partial\left(rF_\theta\right)}{\partial r} - \frac{\partial F_r}{\partial\theta}\right] \tag{17}$$

For a 2D flow in spherical coordinates we get the following expansion of Eqn. (9)

Dispersed phase:

$$\frac{\partial\omega}{\partial t} = k_\nu\left[\frac{1}{r^2}\frac{\partial}{\partial r}\left(r^2\frac{\partial\omega}{\partial r}\right) + \frac{1}{r^2\sin\theta}\frac{\partial}{\partial\theta}\left(\sin\theta\frac{\partial\omega}{\partial\theta}\right) - \frac{\omega}{r^2\sin^2\theta}\right] + \frac{1}{k_\rho}\left[\frac{1}{r}\left(\left(\frac{\partial\left(rF_\theta\right)}{\partial r}\right) - \frac{\partial F_r}{\partial\theta}\right)\right] \tag{18}$$

Continuous phase:

$$\frac{\partial\omega}{\partial t} = k_\nu\left[\frac{1}{e^{3z}}\frac{\partial}{\partial z}\left(e^{z}\frac{\partial\omega}{\partial z}\right) + \frac{1}{e^{2z}\sin\theta}\frac{\partial}{\partial\theta}\left(\sin\theta\frac{\partial\omega}{\partial\theta}\right) - \frac{\omega}{e^{2z}\sin^2\theta}\right] + \frac{1}{k_\rho}\left[\frac{1}{e^{z}}\left(\left(e^{-z}\frac{\partial\left(e^{z}F_\theta\right)}{\partial z}\right) - \frac{\partial F_r}{\partial\theta}\right)\right] \tag{19}$$

The stream function ψ is introduced such that,

$$u_r = -\frac{1}{r^2\sin\theta}\frac{\partial\psi}{\partial\theta} \qquad u_\theta = \frac{1}{r\sin\theta}\frac{\partial\psi}{\partial r} \tag{20}$$

Dispersed phase:

$$\frac{1}{r}\frac{\partial}{\partial r}\left(\frac{1}{\sin\theta}\frac{\partial\psi}{\partial r}\right) + \frac{1}{r^3}\frac{\partial}{\partial\theta}\left(\frac{1}{\sin\theta}\frac{\partial\psi}{\partial\theta}\right) = -\omega \tag{21}$$

continuous phase:

$$\frac{1}{e^{2z}}\frac{\partial}{\partial z}\left(\frac{1}{\sin\theta}e^{-z}\frac{\partial\psi}{\partial z}\right)+\frac{1}{e^{3z}}\frac{\partial}{\partial\theta}\left(\frac{1}{\sin\theta}\frac{\partial\psi}{\partial\theta}\right)=-\omega \tag{22}$$

Equation (10), (11)and (12) are solved to obtain the flow solution.

3.4.2. Boundary conditions for stream function and vorticity:-

$$at \qquad r=0 \qquad u_r=u_\theta=0 \qquad \omega=0 \qquad \psi=0$$

$$at \qquad r=r_{\max} \qquad u_r=u_\theta=0 \qquad \omega=0 \qquad \psi=0$$

$$at \qquad \theta=0 \qquad u_r=0 \qquad \frac{\partial u_r}{\partial\theta}=0 \qquad \omega=0 \qquad \psi=0$$

$$at \qquad \theta=\frac{\pi}{2} \qquad u_r=0 \qquad \frac{\partial u_r}{\partial\theta}=0 \qquad \omega=0 \qquad \psi=0$$

3.5. VOF (f) equation:-

VOF advection equation for incompressible flow:

$$\frac{\partial f}{\partial t^*}+\left(\overrightarrow{u^*}.\nabla^*\right)f=0 \tag{23}$$

By non-dimensionalizing the equation with the factors used in section 2.3 we get:

$$\frac{\partial f}{\partial t}+\mathrm{Re}\left(\vec{u}.\nabla\right)f=0 \tag{24}$$

In spherical coordinates:

$$\frac{\partial f}{\partial t}+\mathrm{Re}\left(\frac{u_r}{r}\frac{\partial f}{\partial \theta}+u_\theta\frac{\partial f}{\partial r}\right)=0 \qquad (25)$$

Eqn. (22) is solved to track the interface it is coupled with Navier-Stokes equation through u_r, u_θ and the properties viscosity and density.

3.5.1 Boundary conditions:-

$$at \quad r=0 \quad f=0 \quad , \quad r=r_{\max} \quad f=1$$
$$\theta=0 \quad \frac{\partial f}{\partial \theta}=0 \quad , \quad \theta=\frac{\pi}{2} \quad \frac{\partial f}{\partial \theta}=0$$

3.6. voltage calculation:

Charge conservation equation:

$$\nabla^*.\overrightarrow{J^*}+\frac{dq^*}{dt^*}=0 \qquad (26)$$

Where, $\overrightarrow{J^*}=\sigma^*\overrightarrow{E^*}+q^*\overrightarrow{u^*}$

Voltage equation is derived from charge conservation equation by assuming charge convection due to the flow field $q\vec{u}$ and the charge accumulation $\frac{dq}{dt}$ to be zero.

$$\nabla^*.\left(\sigma^*\nabla^*V^*\right)=0 \qquad (27)$$

Non-dimensionalization of the Voltage equation:

$$V = \frac{V^*}{V_o} \qquad k_\sigma = \frac{\sigma^*}{\sigma_2} \qquad \nabla = a\nabla^*$$

After Non-dimensionalization the above equation becomes

$$\nabla.\left(k_\sigma \nabla V\right) = 0 \tag{28}$$

Where,

$$k_\sigma = f + (1-f)\frac{\sigma_1}{\sigma_2}$$

Eqn(21) can be expressed in spherical coordinates in the following way:

$$\frac{1}{r^2}\frac{\partial}{\partial r}\left(r^2 k_\sigma \frac{\partial V}{\partial r}\right) + \frac{1}{r^2 \sin\theta}\frac{\partial}{\partial \theta}\left(r^2 k_\sigma \sin\theta \frac{\partial V}{\partial r}\right) = 0 \tag{29}$$

Where k_σ is the conductivity ratio.

3.6.1 Boundary conditions:

$$at \quad r = 0 \quad V = 0 \quad , \quad r = r_{\max} \quad V = \cos(\omega t)$$

3.6.2 Electric field:

$$\overrightarrow{E^*} = -\nabla^* V^* \tag{30}$$

Non-dimensionalization of the above equation:

$$\vec{E} = \frac{E^*}{E_o} \qquad \nabla = a\nabla^* \qquad V = \frac{V^*}{V_o}$$

$$\vec{E} = -\frac{aV_o}{E_o}\nabla V$$

We define

$$E_o = \frac{V_o}{R_\infty}$$

Eqn. (20) becomes,

$$\vec{E} = -R_\infty a \nabla V \tag{31}$$

3.7. Shear stress due to electric field:

Shear stress due to electric field acting on the interface of the droplet along normal and tangential direction from (Taylor 1966),

$$nn_E = \frac{k_1^*}{8\pi}\left(E_{1n}^{*2} - E_{1t}^{*2}\right) - \frac{k_2^*}{8\pi}\left(E_{2n}^{*2} - E_{2t}^{*2}\right) \tag{32}$$

$$n\theta_E = \frac{E_{1t}^*}{4\pi}\left(k_1^* E_{1n}^* - k_2^* E_{2n}^*\right) \tag{33}$$

Where, $E_n = \vec{E}.n = \left(E_r \hat{r} + E_\theta \theta\right).\left(n_r \hat{r} + n_\theta \theta\right) = E_r n_r + E_\theta n_\theta$

$E_t = \vec{E}.\hat{t} = \left(E_r \hat{r} + E_\theta \hat{\theta}\right).\left(t_r \hat{r} + t_\theta \hat{\theta}\right) = E_r t_r + E_\theta t_\theta$

3.8. Forces acting at the interface:

The surface tension force and the force due to electric field acting at the interface are surface forces, these surface forces are converted in to volume forces using CSF model approach which eliminates the need of interface reconstruction (Hirt and Nichols 1981, Aulisa et al., 2006) to apply the forces accurately at the interface.

From (Brackbill et al., 1990), for any surface force at the interface, volume force is evaluated as:

$$\overrightarrow{F_V} = |\overrightarrow{F_A}| \frac{\nabla \tilde{c}(\vec{x})}{[c]} \qquad (34)$$

3.8.1. Surface tension force:

Surface tension force acts only in the normal direction with respect to the interface since there is no gradient in surface tension coefficient (γ) along the tangential direction.

$$\overrightarrow{F_{SV}^*} = |\overrightarrow{F_{SA}^*}| \frac{\nabla f(\vec{x})}{[f]} \qquad (35)$$

($\tilde{c}(\vec{x}) = f(\vec{x})$)

f is a smoothed value(non-linear)

$$|\overrightarrow{F_{SA}^{*}}| = \gamma\kappa(\vec{x}) \tag{36}$$

Non dimensional surface tension force:

$$\overrightarrow{F_{SV}} = \frac{\left|\overrightarrow{F_{SA}^{*}}\right| \frac{\nabla f(\vec{x})}{[f]}}{\mu U \big/ a^2} = \frac{a^2\gamma\kappa}{\mu U}\frac{\nabla f(\vec{x})}{[f]} \tag{37}$$

We define the capillary number as

$$\mathrm{Ca} = \frac{\mu U}{\gamma} \text{ ,}$$

Capillary number gives the relative strength of viscous force over the surface tension force, hence by considering different values of the Capillary number we can study different systems that correspond to different magnitude of surface tension force $\overrightarrow{F_{SV}}$ relative to the viscous force

$$\overrightarrow{F_{SV}} == \frac{a^2\kappa(\vec{x})}{ca}\frac{\nabla f(\vec{x})}{[f]} \quad , \quad \kappa = -\nabla.\hat{n} \tag{38}$$

The curvature is calculated using an ALE like scheme (Brackbill et al. 1990)

Spherical coordinates:

$$\overrightarrow{F_{SV}} = \frac{a^2\kappa(\vec{x})}{ca[f]}\left[\frac{1}{r}\frac{\partial f}{\partial\theta}\theta + \frac{\partial f}{\partial r}\hat{r}\right] \tag{39}$$

$$\kappa(\vec{x}) = \left[\frac{1}{r}\frac{\partial n_\theta}{\partial\theta} + \frac{\partial n_r}{\partial r}\right] \tag{40}$$

3.8.2.Electric force:

Electric force acting on the interface in the normal direction:

$$\overrightarrow{F^*_{EVn}} = |\overrightarrow{F^*_{EAn}}| \frac{\nabla f(\vec{x})}{[f]}$$

$$|\overrightarrow{F^*_{EAn}}| = |nn_E|$$

Non dimensional electric stress acting in the normal direction

$$\overrightarrow{F_{EVn}} = \frac{\left|\overrightarrow{F^*_{EAn}}\right| \frac{\nabla f(\vec{x})}{[f]}}{\mu U / a^2} = \frac{a^2 |nn_E|}{\mu U} \frac{\nabla f(\vec{x})}{[f]}$$

$$= \frac{a^2}{\mu U}\left[\frac{k_1^*}{8\pi}\left(E_{1n}^{*2} - E_{1t}^{*2}\right) - \frac{k_2^*}{8\pi}\left(E_{2n}^{*2} - E_{2t}^{*2}\right)\right]\frac{\nabla f(\vec{x})}{[f]} \qquad (38)$$

Now,

$$E^* = EE_o$$

$$k_{di} = \frac{k_1^*}{k_2^*}$$

$$\overrightarrow{F_{EVn}} = \frac{a^2 k_2^* E_o^2}{\mu U 8\pi}\left[k_{di}\left(E_{1n}^2 - E_{1t}^2\right) - \left(E_{2n}^2 - E_{2t}^2\right)\right]\frac{\nabla f(\vec{x})}{[f]} \qquad (39)$$

$$Ce = \frac{a^2 k_2^* E_o^2}{\mu U}$$

Ce gives the relative strength of electric force over the viscous force

Spherical coordinates:

$$\overrightarrow{F_{EVn}} = \frac{Ce}{8\pi[f]}\left[k_{di}\left(E_{1n}^2 - E_{1t}^2\right) - \left(E_{2n}^2 - E_{2t}^2\right)\right]\left[\frac{1}{r}\frac{\partial f}{\partial \theta}\theta + \frac{\partial f}{\partial r}\hat{r}\right] \tag{40}$$

Similarly Electric force acting in the tangential direction:

$$\overrightarrow{F_{EV\theta}} = \frac{Ce}{4\pi[f]}\frac{E_{1t}}{}\left(k_{di}E_{1n} - E_{2n}\right)\left[\frac{1}{r}\frac{\partial f}{\partial \theta}\theta + \frac{\partial f}{\partial r}\hat{r}\right] \tag{41}$$

u_θ

We define,

$$\mathrm{Ca}_E = \mathrm{Ca}\times\mathrm{Ce}$$
$$= \frac{a^2 k_2^* E_o^2}{\gamma}$$

Ca_E, gives the relative strength of Electric force over the surface tension force**.** The current study is based on the parameters (Ca_E **,** Ca **,** Ce)

3.9 . Lagrangian particle tracking:

The x and y coordinate or the position of the particle is tracked using the following basic equation of kinematics

$$\frac{d\overrightarrow{x^*}}{dt^*} = \overrightarrow{u^*} \tag{42}$$

By non-dimensionalizing the above equation using the factors used in section 2.3 we get:

$$\frac{d\vec{x}}{dt} = \mathrm{Re}\,\vec{u} \tag{43}$$

The numerical procedure to track the particle with respect to time is discussed elaborately in chapter 4.

CHAPTER 4

NUMERICAL METHODOLOGY

4.1. Discretization:

4.1.1. Vorticity equation:

$$\frac{\partial \omega}{\partial t} = k_\nu \left[\frac{1}{r^2} \frac{\partial}{\partial r} \left(r^2 \frac{\partial \omega}{\partial r} \right) + \frac{1}{r^2 \sin\theta} \frac{\partial}{\partial \theta} \left(\sin\theta \frac{\partial \omega}{\partial \theta} \right) - \frac{\omega}{r^2 \sin^2\theta} \right] + \frac{1}{k_\rho} \left[\frac{1}{r} \left(\left(\frac{\partial (r F_\theta)}{\partial r} \right) - \frac{\partial F_r}{\partial \theta} \right) \right] \tag{44}$$

A central difference scheme is adopted to discretize the spatial derivatives with a second order accuracy and the vorticity equation is integrated with an ADI scheme. The electric and surface tension forces are treated explicitly which gives rise to a stability criteria restricting the time step to very low values of the order 10^{-6}. The forces can be calculated implicitly eliminating the need of very low time step, but the hurdles in implementing an implicit approach demands to adopt an explicit treatment in the current study.

$$\frac{\partial \omega}{\partial t} = \frac{\omega_{R,t}^{n+\frac{1}{2}} - \omega_{R,t}^{n}}{\Delta t / 2} \tag{45}$$

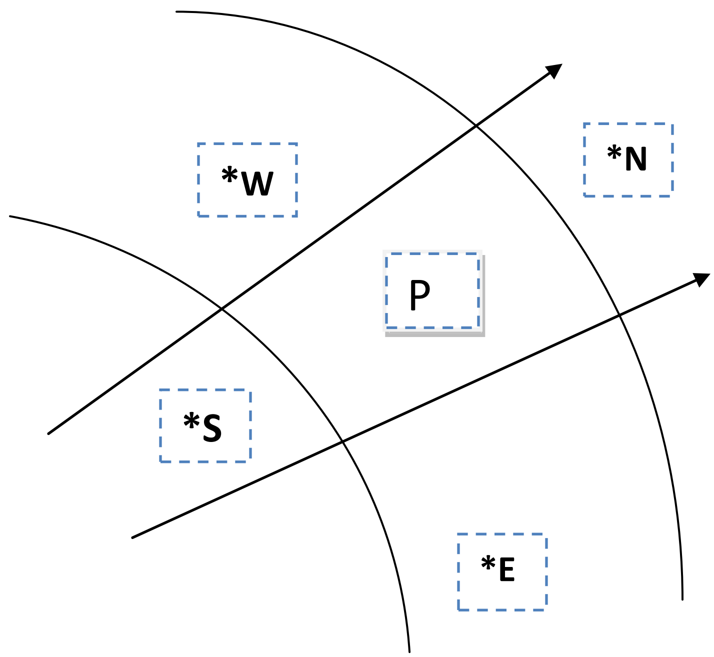

Figure 5. Stencil

$$\frac{k_\nu}{r^2}\frac{\partial}{\partial r}\left(r^2\frac{\partial \omega}{\partial r}\right)=\frac{k_\nu}{r_{R,t}^2}\left[\frac{r_{R+\frac{1}{2},t}^2(\omega_{R+1,t}^{n+\frac{1}{2}}-\omega_{R,t}^{n+\frac{1}{2}})-r_{R-\frac{1}{2},t}^2(\omega_{R,t}^{n+\frac{1}{2}}-\omega_{R-1,t}^{n+\frac{1}{2}})}{\Delta r^2}\right] \tag{46}$$

$$\frac{k_\nu}{r^2\sin\theta}\frac{\partial}{\partial\theta}\left(\sin\theta\frac{\partial\omega}{\partial\theta}\right)=\frac{k_\nu}{r_{R,t}^2\sin\theta_{R,t}}\left[\frac{\sin\theta_{R,t+\frac{1}{2}}(\omega_{R,t+1}^{n+\frac{1}{2}}-\omega_{R,t}^{n+\frac{1}{2}})-\sin\theta_{R,t-\frac{1}{2}}(\omega_{R,t}^{n+\frac{1}{2}}-\omega_{R,t-1}^{n+\frac{1}{2}})}{\Delta\theta^2}\right] \tag{47}$$

$$\frac{\omega}{r^2\sin^2\theta}=\frac{\omega_{R,t}}{r_{R,t}^2\sin\theta_{R,t}} \tag{48}$$

$$\frac{1}{k_\rho}\left[\frac{1}{r}\frac{\partial(rF_\theta)}{\partial r}-\frac{\partial F_r}{\partial\theta}\right]=\frac{1}{r_{R,t}}\frac{\left[F_{R,t+1}^n-F_{R,t-1}^n\right]}{2\Delta\theta}+\frac{1}{r_{R,t}}\frac{\left[r_{R+\frac{1}{2},t}(F_{R,t+1}^n+F_{R,t}^n)-r_{R-\frac{1}{2},t}(F_{R,t}^n+F_{R,t-1}^n)\right]}{2\Delta r} \tag{49}$$

Eqn. (41) after discretization can be written as:

$$a_P\omega_p=a_S\omega_S+a_N\omega_N+a_W\omega_W+a_E\omega_E+S \tag{50}$$

Where,

$$a_P = a_S + a_N + a_W + a_E + \frac{k_\nu \Delta\theta \Delta r}{\sin\theta_p} + \frac{k_\nu \sin\theta_p \Delta\theta \Delta r r_p^2}{\Delta t/2} \tag{51}$$

$$a_N = \frac{k_\nu \sin\theta_p \Delta\theta r_n^2}{\Delta r} \quad a_S = \frac{k_\nu \sin\theta_p \Delta\theta r_s^2}{\Delta r} \quad a_W = \frac{k_\nu \sin\theta_p \Delta r r_w^2}{\Delta\theta} \quad a_E = \frac{k_\nu \sin\theta_p \Delta r r_e^2}{\Delta\theta}$$

4.1.2. Stream function equation:

$$\frac{1}{r}\frac{\partial}{\partial r}\left(\frac{1}{\sin\theta}\frac{\partial\psi}{\partial r}\right) + \frac{1}{r^3}\frac{\partial}{\partial\theta}\left(\frac{1}{\sin\theta}\frac{\partial\psi}{\partial\theta}\right) = -\omega \tag{52}$$

$$\frac{1}{r}\frac{\partial}{\partial r}\left(\frac{1}{\sin\theta}\frac{\partial\psi}{\partial r}\right) = \frac{r_{R,t}\Delta\theta}{1}\left[\frac{(\psi_{R+1,t} - \psi_{R,t}) - (\psi_{R,t} - \psi_{R-1,t})}{\Delta r}\right] \tag{53}$$

$$\frac{1}{r^3}\frac{\partial}{\partial\theta}\left(\frac{1}{\sin\theta}\frac{\partial\psi}{\partial\theta}\right) = \frac{\sin\theta_{R,t}\Delta r}{r_{R,t}\Delta\theta}\left[\frac{1}{\sin\theta_{R,t+1/2}}(\psi_{R,t+1} - \psi_{R,t}) + \frac{1}{\sin\theta_{R,t-1/2}}(\psi_{R,t} - \psi_{R,t-1})\right] \tag{54}$$

The above equations can be represented in the given form:

$$a_P\psi_p = a_S\psi_S + a_N\psi_N + a_W\psi_W + a_E\psi_E - \omega_p r_p^2 \sin\theta\Delta\theta\Delta r \tag{55}$$

Where,

$$a_P = a_S + a_N + a_W + a_E \tag{56}$$

Stream function equations are elliptic equations solved by a line by line TDMA approach.

4.1.3 VOF advection equation:

An explicit upwind scheme is used to advect the volume fraction advection equation in time and space. Upwind schemes use an adaptive or solution-sensitive finite difference stencil to numerically simulate more properly the direction of propagation of information in a flow field. The spatial derivatives are evaluated using a forward or backward difference depending on the signs of the velocities in both r and θ direction.

$$\frac{\partial f}{\partial t}+\mathrm{Re}\left(\frac{u_r}{r}\frac{\partial f}{\partial\theta}+u_\theta\frac{\partial f}{\partial r}\right)=0 \tag{57}$$

$$\mathrm{F}_r^-=\left[\frac{\mathrm{f}_{R,t}^n\text{-}\mathrm{f}_{R-1,t}^n}{\Delta r}\right]\qquad \mathrm{F}_r^+=\left[\frac{\mathrm{f}_{R+1,t}^n\text{-}\mathrm{f}_{R,t}^n}{\Delta r}\right]\qquad \mathrm{F}_t^-=\left[\frac{\mathrm{f}_{R,t-1}^n\text{-}\mathrm{f}_{R,t}^n}{r_{R,t}\Delta\theta}\right]$$

$$\mathrm{F}_t^+=\left[\frac{\mathrm{f}_{R,t+1}^n\text{-}\mathrm{f}_{R,t}^n}{r_{R,t}\Delta\theta}\right] \tag{58}$$

Derivatives:

$$\mathrm{D\_t}=\Delta t\left[\max(\mathrm{u}_\theta,0)\mathrm{F}_t^-+\min(\mathrm{u}_\theta,0)\mathrm{F}_t^+\right] \tag{59}$$

$$\mathrm{D\_r}=\Delta t\left[\max(\mathrm{u}_r,0)\mathrm{F}_r^-+\min(\mathrm{u}_r,0)\mathrm{F}_r^+\right] \tag{60}$$

VOF advection equation after discretization:

$$f_{R,t}^{n+1} = f_{R,t}^{n} - \mathrm{Re}\left[\mathrm{D\_t} + \mathrm{D\_r}\right] \tag{61}$$

4.1.4. Voltage equation:

$$\frac{1}{r^2}\frac{\partial}{\partial r}\left(r^2 k_\sigma \frac{\partial V}{\partial r}\right) + \frac{1}{r^2 \sin\theta}\frac{\partial}{\partial \theta}\left(r^2 k_\sigma \sin\theta \frac{\partial V}{\partial r}\right) = 0 \tag{62}$$

The above equation is discretized spatially using a central difference scheme with a second order accuracy

$$\frac{1}{r^2}\frac{\partial}{\partial r}\left(r^2 k_\sigma \frac{\partial V}{\partial r}\right) = \left[\frac{r_{R+\frac{1}{2},t}^2 k_{\sigma R+\frac{1}{2},t}}{r_{R,t}^2 \Delta r^2} V_{R+!,t} + \frac{r_{R-\frac{1}{2},t}^2 k_{\sigma R-\frac{1}{2},t}}{r_{R,t}^2 \Delta r^2} V_{R-1,t}\right] - \left[\frac{r_{R+\frac{1}{2},t}^2 k_{\sigma R+\frac{1}{2},t}}{r_{R,t}^2 \Delta r^2} + \frac{r_s^2 r_{R-\frac{1}{2},t}^2 k_{\sigma R-\frac{1}{2},t}}{r_{R,t}^2 \Delta r^2}\right] V_{R,t} \tag{63}$$

$$\frac{1}{r^2 \sin\theta}\frac{\partial}{\partial \theta}\left(k_{di} \sin\theta \frac{\partial V}{\partial r}\right) = \left[\frac{\sin\theta_{R,t+\frac{1}{2}} k_{diR,t+\frac{1}{2}}}{r_{R,t}^2 \sin\theta_{R,t} \Delta\theta^2} V_{R,t+1} + \frac{\sin\theta_{R,t-\frac{1}{2}} k_{diR,t-\frac{1}{2}}}{r_{R,t}^2 \sin\theta_{R,t} \Delta\theta^2} V_{R,t-1}\right] - \left[\frac{\sin\theta_{R,t+\frac{1}{2}} k_{diR,t+\frac{1}{2}}}{r_{R,t}^2 \sin\theta_{R,t} \Delta\theta^2} + \frac{\sin\theta_{R,t-\frac{1}{2}} k_{R,t-\frac{1}{2}}}{r_{R,t}^2 \sin\theta_{R,t} \Delta\theta^2}\right] V_{R,t} \tag{64}$$

Eqn(60) can be written in the form

$$a_P V_p = a_S V_S + a_N V_N + a_W V_W + a_E V_E \tag{65}$$

Where,

$$a_P = a_S + a_N + a_W + a_E \tag{66}$$

Voltage equations are solved similar to the stream function equation using a TDMA approach for faster convergence.

4.1.5 Lagrangian particle tracking:

$$\frac{d\vec{x}}{dt} = \vec{u} \tag{67}$$

The governing equation (Eqn. 64) for particle trajectory is integrated using a fourth order Runge Kutta method. RK_4 (fourth order Runge Kutta) method is chosen to track the exact location of the particle at a particular time with higher accuracy. The velocity field $\vec{u}$ is obtained from the flow solution, $\vec{u_i}$ is evaluated from $\vec{u}$ at a particular locations of $\vec{x}$ and t with a cubic interpolation technique.

$$\vec{k_1} = \Delta t * \vec{u_i}\left(t_o,\ \vec{x_o} \right) \tag{68}$$

$$\vec{k_2} = \Delta t * \vec{u_i}\left(t_o + \Delta t/2, \vec{x_o} + \vec{k_1}/2 \right) \tag{69}$$

$$\vec{k_3} = \Delta t * \vec{u_i}\left(t_o + \Delta t/2,\ \vec{x_o} + \vec{k_2}/2 \right) \tag{70}$$

$$\vec{k_4} = \Delta t * \vec{u_i}\left(t_o + \Delta t,\ \vec{x}_o + \vec{k}_3 \right) \tag{71}$$

$\vec{k_1}$, $\vec{k_2}$, $\vec{k_3}$, $\vec{k_4}$ are obtained using the interpolated value $\vec{u_i}$

The new position is calculated from $\vec{k_1}$, $\vec{k_2}$, $\vec{k_3}$, $\vec{k_4}$ and old position $\vec{x}_o$

$$\vec{x} = \vec{x}_o + \left(\overrightarrow{k_1} + 2\overrightarrow{k_2} + 2\overrightarrow{k_3} + \overrightarrow{k_4} \right) / 6 \tag{72}$$

4.1.6. Solution algorithm:

- Initialize the variables ψ , ω , f , V at time t=0.
- Calculate u_r and u_θ using the initial values of ψ
- Solve the volume fraction advection equation explicitly to obtain volume fraction f using the values of u_r and u_θ .
- Calculate density k_ρ and k_ν using f .
- Solve the voltage equation to obtain the voltage solution and the Electric field at the interface.
- Calculate the forces (Electrical and surface tension) acting at the interface using CSF approach.
- Solve for the vorticity using the vorticity transport equation using the calculated interfacial forces at step 5 as the source till convergence is achieved.
- Solve for stream-function using the stream function equation with the vorticity calculated at step 6 as the source till convergence is achieved.
- Go to step 1 till the required time has reached.

CHAPTER 5

RESULTS AND DISCUSSION

5.1. Validation of the numerical model:

The model is validated by comparing results for the limiting case with no deformation where analytical results are available in published literature. The solutions for the stream function and vorticity profile inside and outside the droplet are obtained numerically and compared with Taylor's (1966) analytical solution as shown in Fig. 6 and Fig. 7

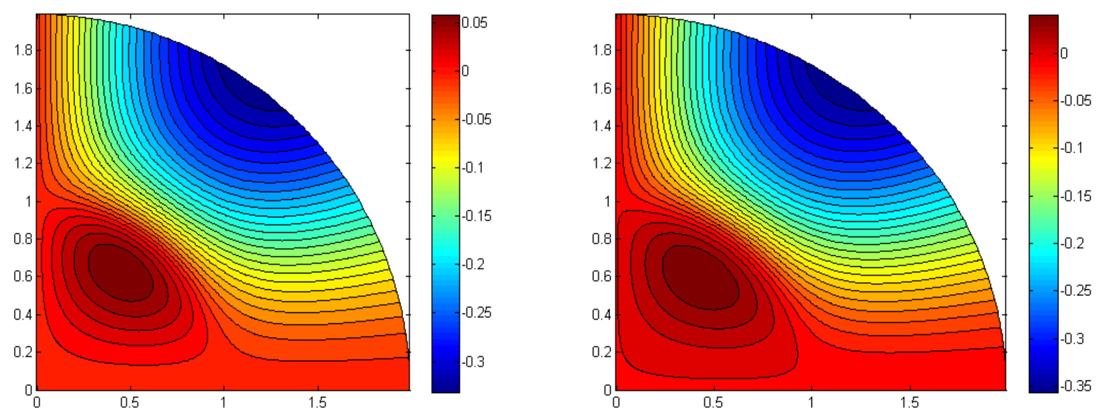

Figure 6. Streamlines inside and outside a drop with no deformation Taylor's analytical solution (left) and numerical prediction (right)

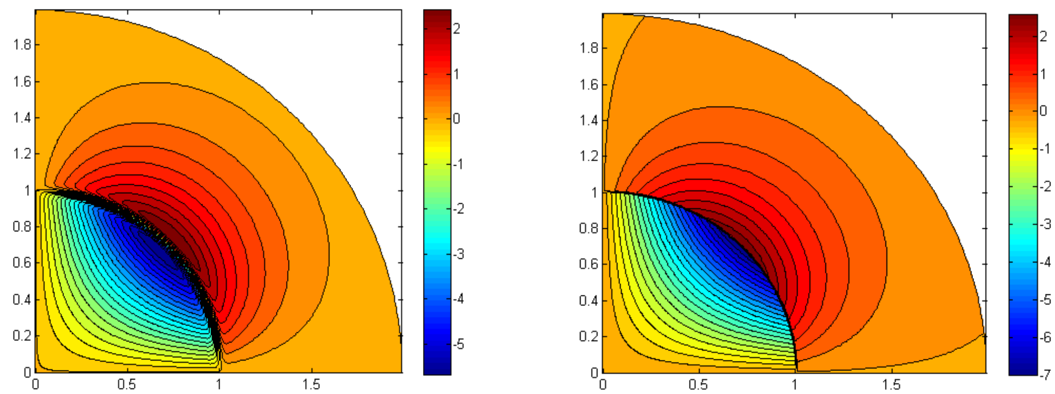

Figure 7. Vorticity inside and outside a drop with no deformation numerical prediction (left) and Taylor's analytical solution (right)

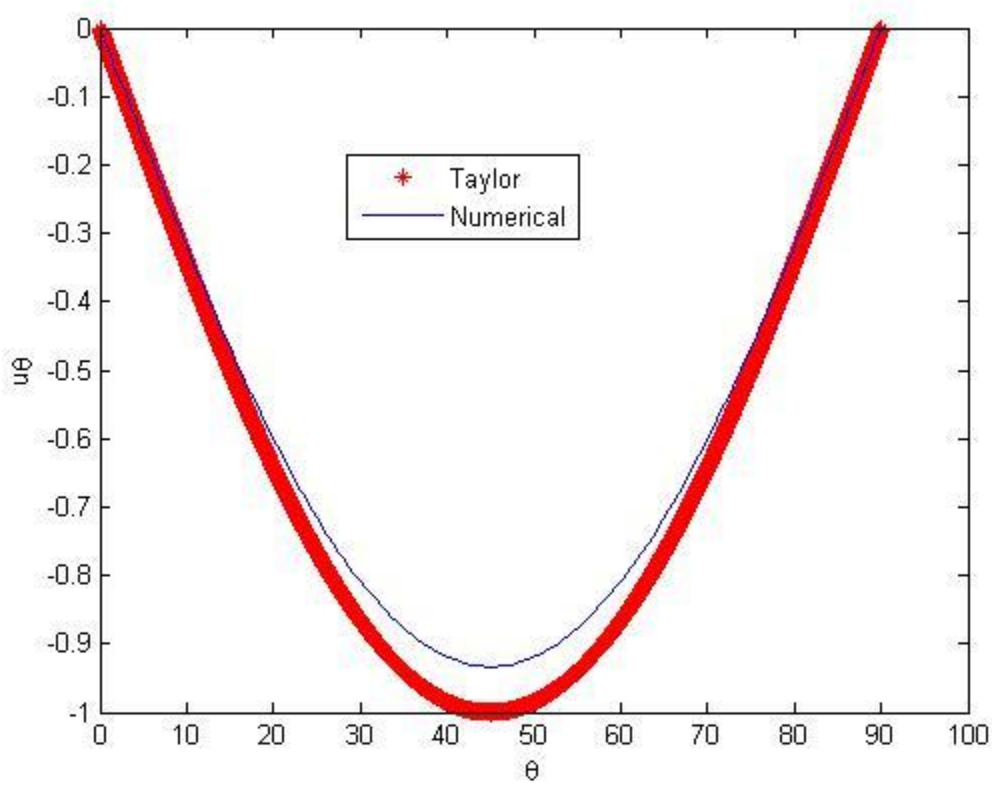

Figure 8. Variation of u_θ for analytical and numerical solutions on the drop surface R=1 along θ-direction

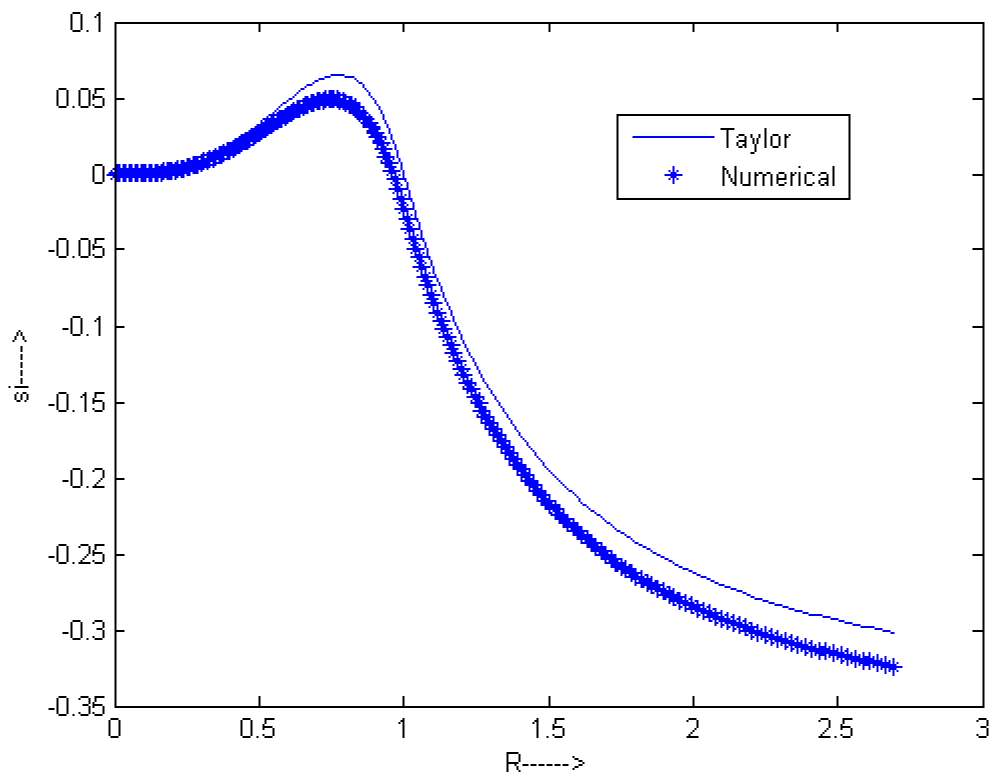

Figure 9. Variation of ψ for the analytical and numerical solution along r-direction at $\theta = 45^o$

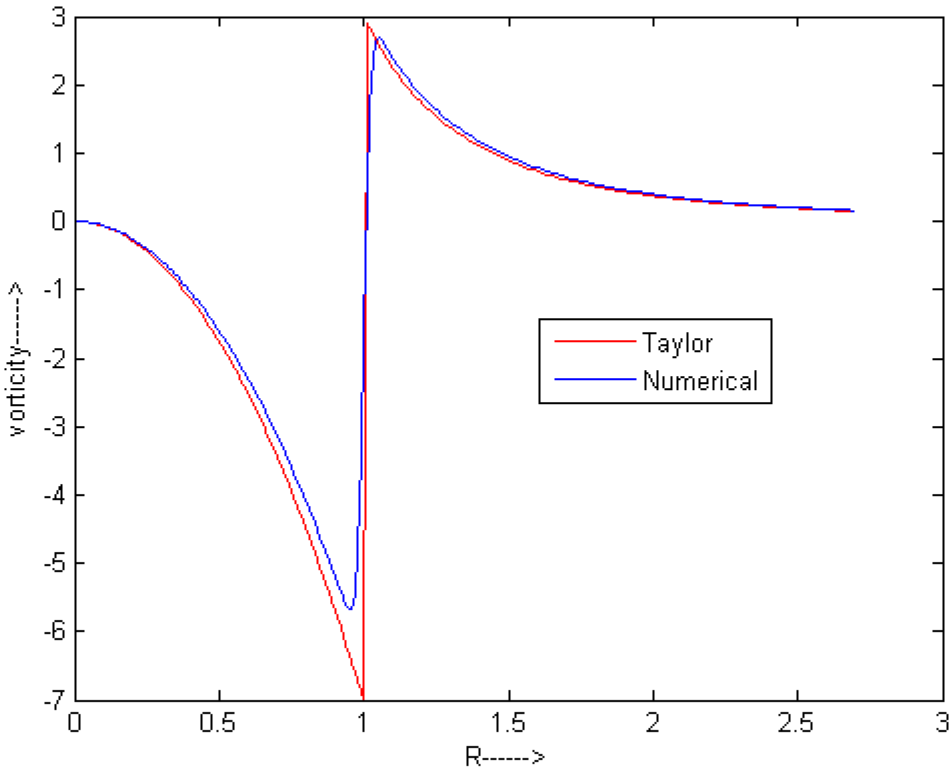

Figure 10. Variation of ω for Taylor's analytical solution and numerical solution by present model along r-direction at $\theta = 45^o$

In Fig. 9 and 10, stream function and vorticity values are plotted along the r-direction at $\theta = 45^o$ respectively. The results indicated that the stream function and vorticity values obtained numerically matches with the analytical solution proposed by Taylor with an offset average error of 0.05% and 0.1% respectively.

	Taylor (1966)	Numerical model
Maximum velocity at the interface	1.0	0.95

Table.1.Maximum velocity at the interface from Taylor's solution and the numerical model

In Figure 8, Tangential velocity is plotted at the interface R=1 along the θ-direction, The results indicated that the numerical model predicted the maximum surface velocity to be at $\theta = 45$ and the value to be 0.95 as shown in the table above which is in close agreement with Taylor's (1966) analytical solution with error less than 5%.

5.2. Results:

Results are obtained for two electric capillary numbers Ca_E = 40, 80 and a range of dimensionless frequencies ν =5, 15 and 50 with a fixed Ca_E =80. The flow Reynolds number (Re) and other physical properties are kept constant as shown in the table.

Cases:

Ce	Ca	Ca_E	q=k1/k2	Frequency (ν)	Re	Viscosity ratio(k_ν)	Density ratio(k_ρ)	Conductivity Ratio(R)
1000	0.08	80	0.0019	5	1	1	1	0.03125
500	0.08	40	0.0019	5	1	1	1	0.03125
1000	0.08	80	0.0019	15	1	1	1	0.03125
1000	0.08	80	0.0019	50	1	1	1	0.03125

Table 2. Cases simulated in the current work

5.3. Study of flow field for Ca_E = 80, dimensionless frequency = 5

In Figure11, the transient voltage fields for Ca_E = 80 and $\nu = 5$ are plotted. The alternating voltage is given in the form of a sine wave $V = V_o \sin\phi$, where $\phi = \omega t$. The voltage field plotted for different times corresponds to $\phi = 0, \pi/2, \pi, 3\pi/2, 2\pi$ on the sine wave $V = V_o \sin\phi$ as shown in Figure 8. It is observed that the voltage field repeats after 1 sine cycle that is at $\phi = \pi$.

On the contrary, the flow field or the velocity vector field plotted at different times as shown in Figures12-15, repeats at $\phi = \pi$ which is ½ of a sine cycle. The change in the time period of both the fields can be attributed to the electric normal stress behavior at theta = 0 and theta = pi/2 plotted against the time in Fig.16 and Fig.17 respectively. It is observed from Fig.16 and Fig.17 that the normal stress which is a function of voltage or the electric field shows the same behavior after a ½ sine cycle irrespective of the change in sign of the voltage after a ½ cycle.

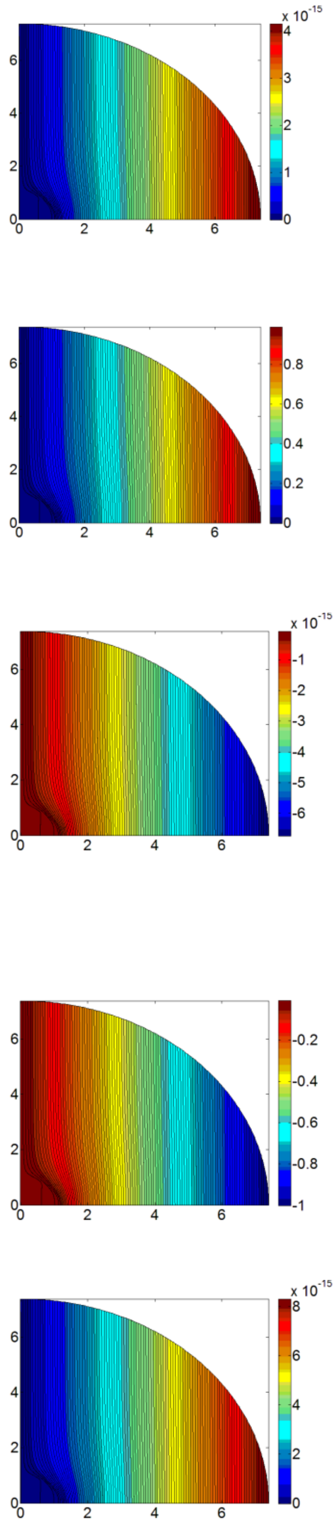

Figure 11. Contours of the voltage field at different times corresponding to $\phi = 0, \frac{\pi}{2}, \pi, \frac{3\pi}{2}, 2\pi$

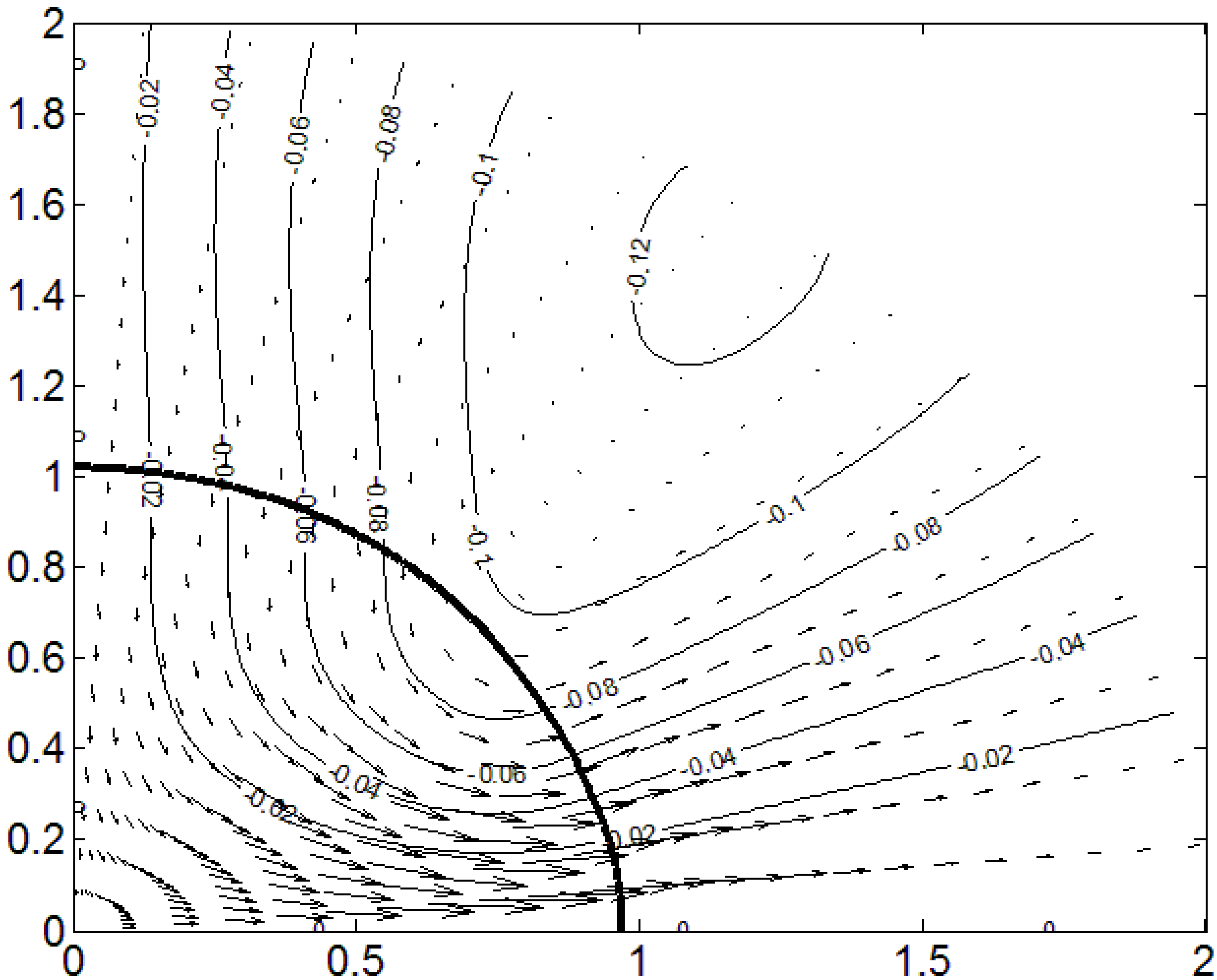

Figure 12. Velocity vector field and streamlines for $Ca_E = 80$, $\nu = 5$ at t=0 or $\phi = 0$

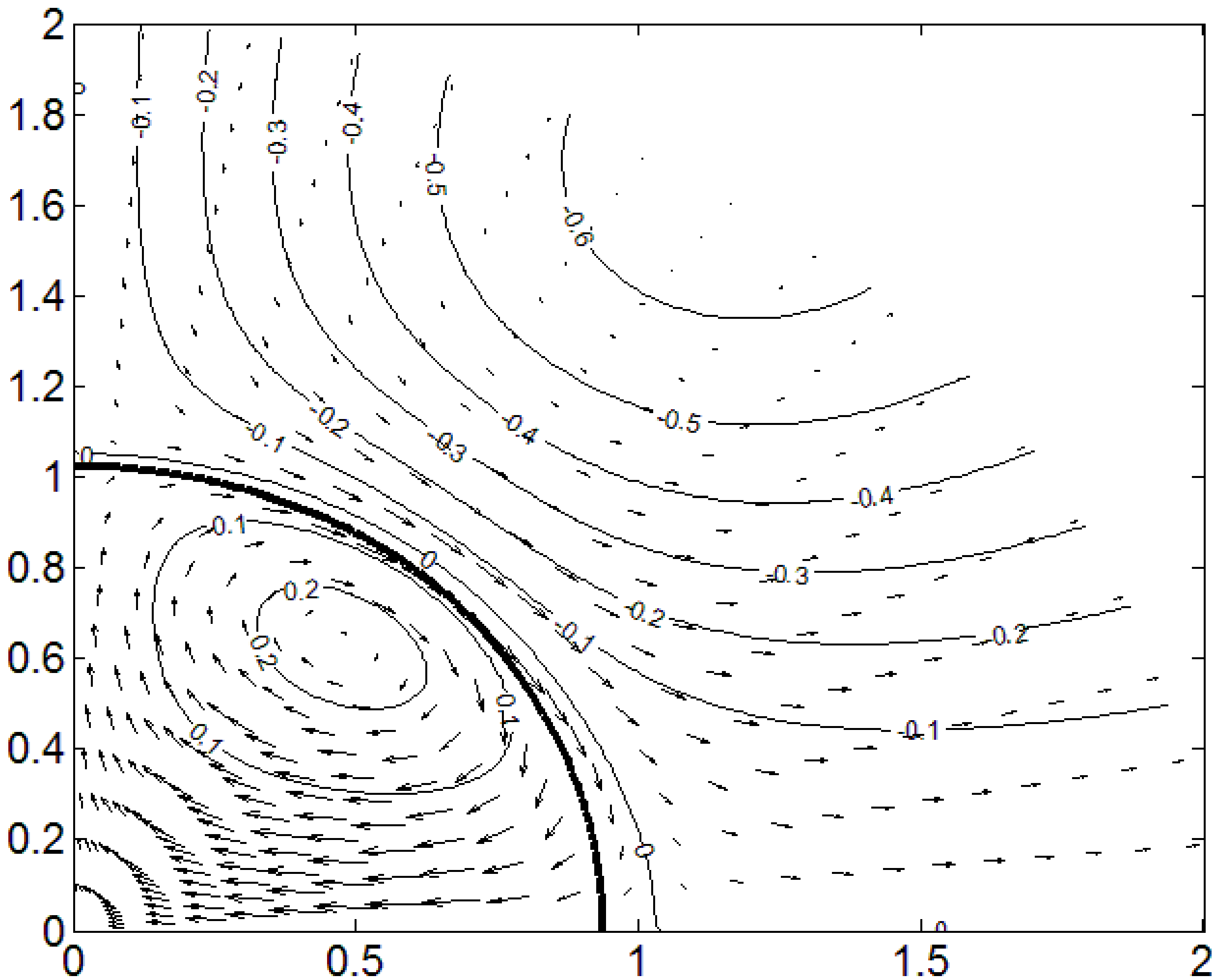

Figure 13. Velocity vector field and streamlines for $Ca_E = 80$, $\nu = 5$ at t=0.05 or $\phi = \frac{\pi}{2}$

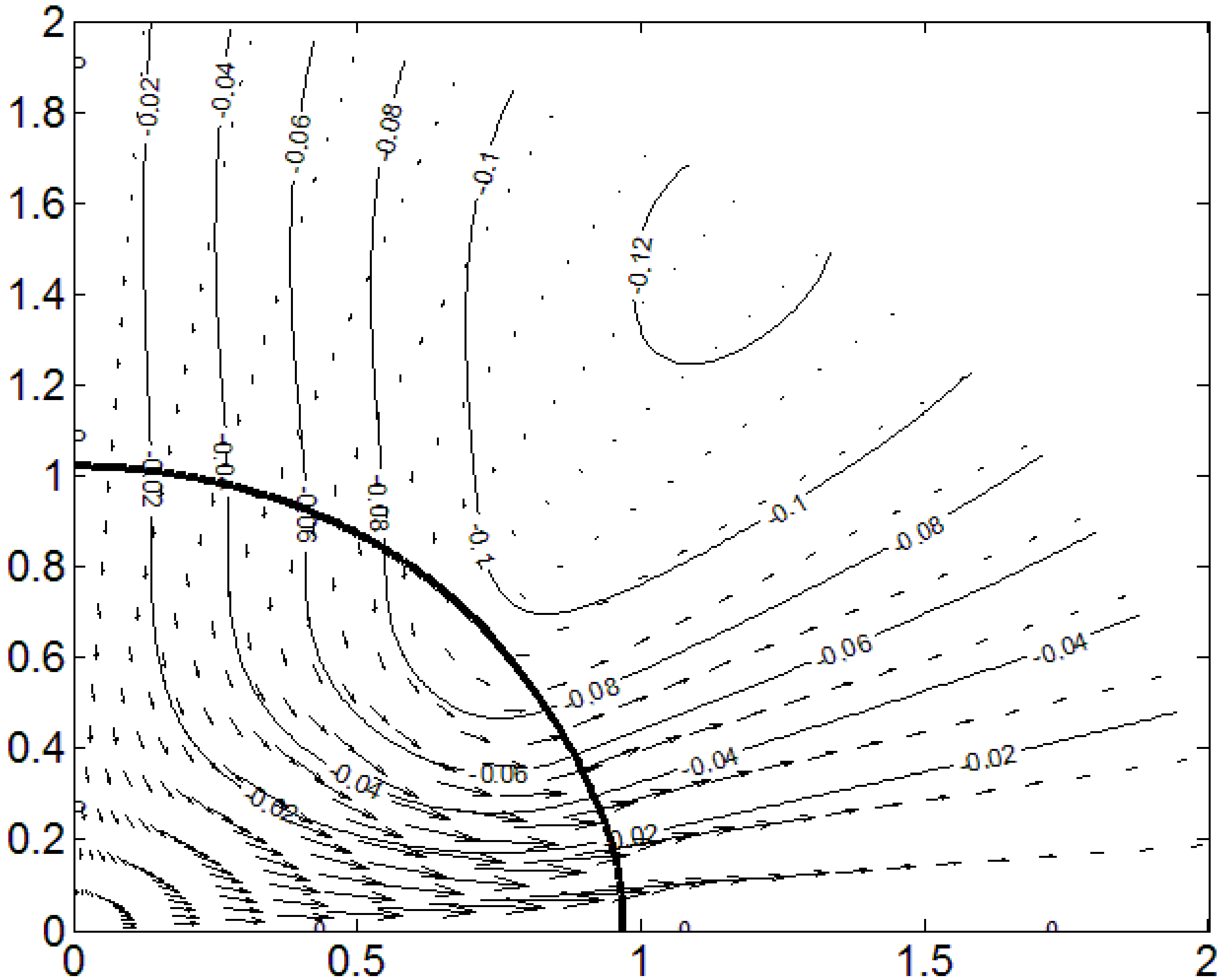

Figure 14. Velocity vector field and streamlines for $Ca_E = 80$ at t=0.1 or $\phi = \pi$

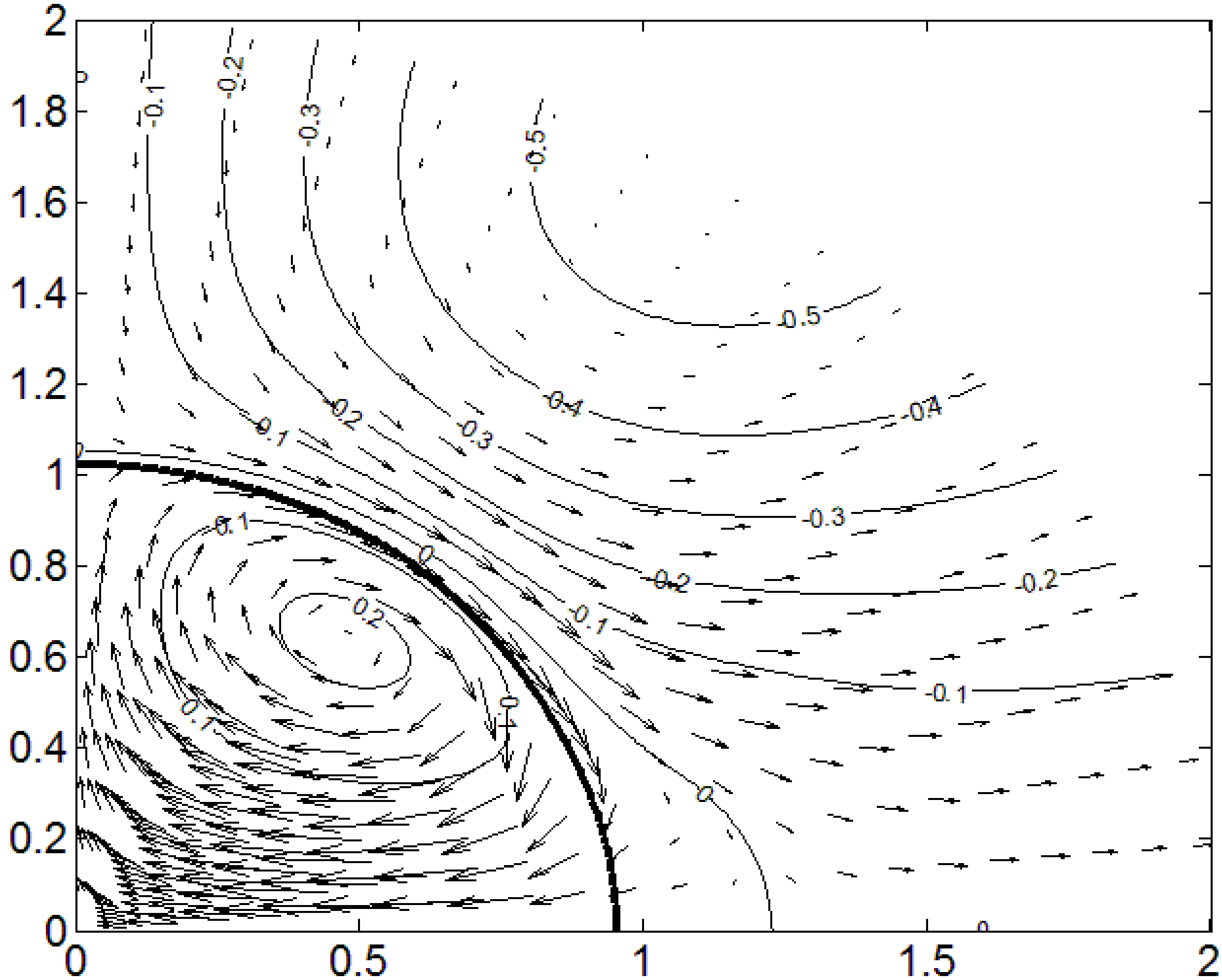

Figure 15. Velocity vector field and streamlines for $Ca_E = 80$ at t=0.15 or $\phi = \frac{3\pi}{2}$

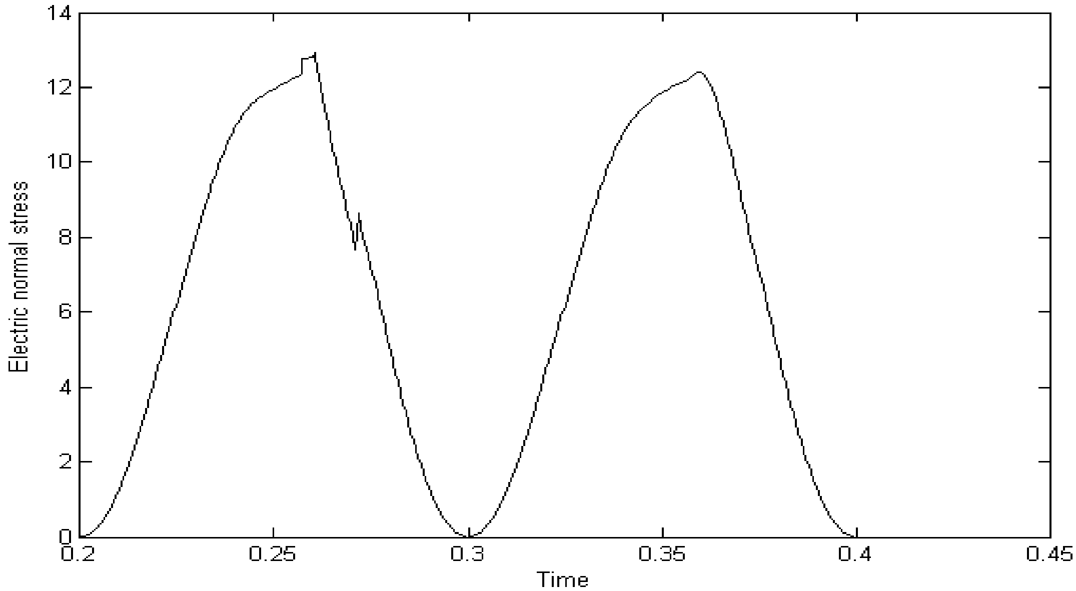

Figure 16. Normal stress at the interface, $\theta = \frac{\pi}{2}$ with time for one cycle, $Ca_E = 80$, $\nu = 5$

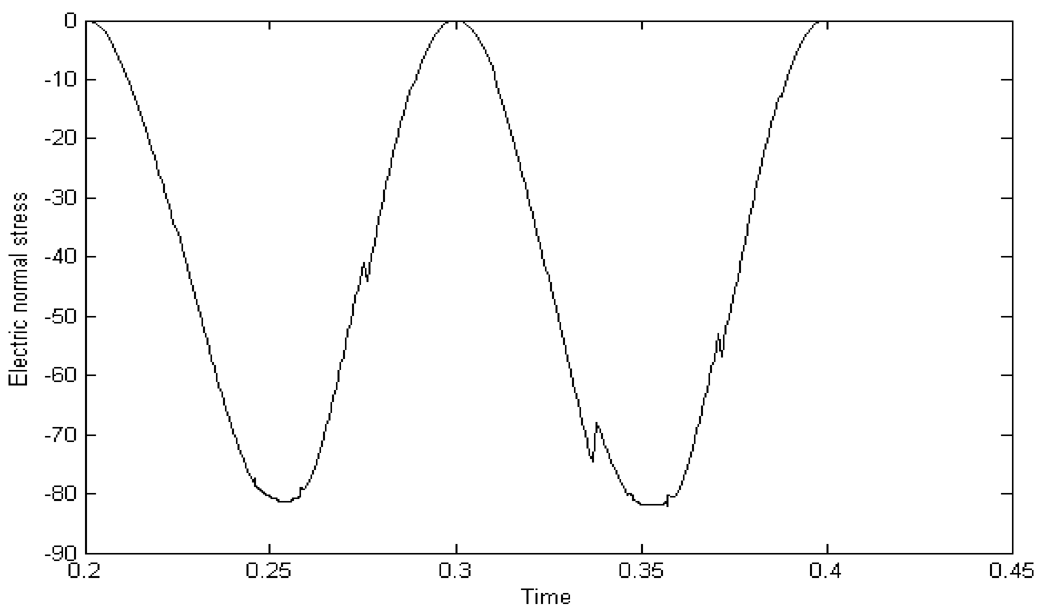

Figure 17. Normal stress at the interface, $\theta = 0$ with time for one cycle, $Ca_E = 80$, $\nu = 5$

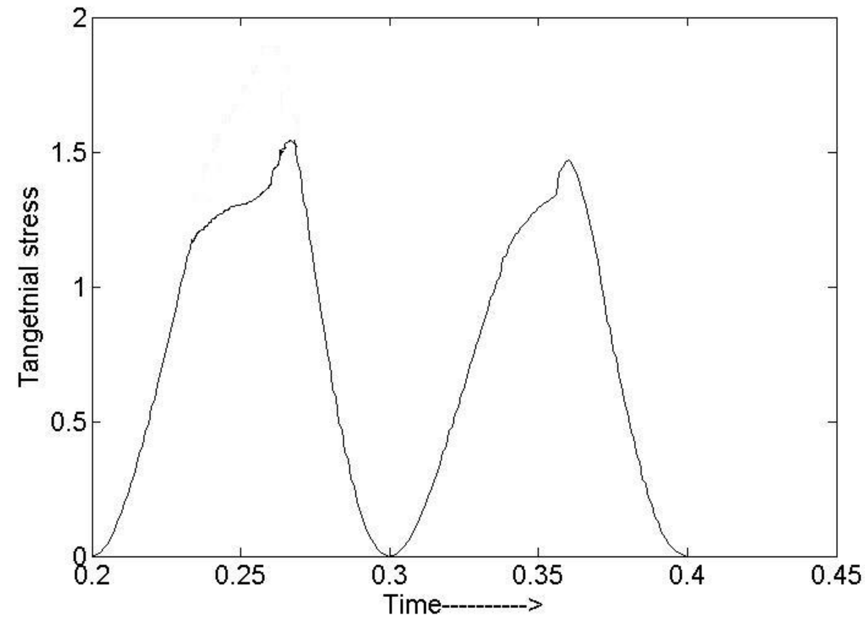

Figure 18. Tangential stress at the interface, $\theta = \dfrac{\pi}{2}$ with time for one cycle, $Ca_E = 80$, $\nu = 5$

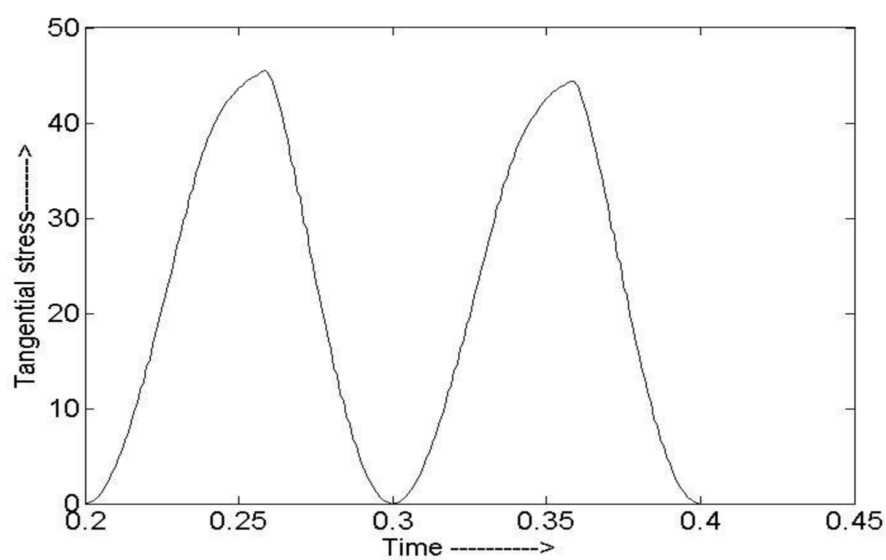

Figure 19. Tangential stress at the interface, $\theta = 0$ with time for one cycle, $Ca_E = 80$, $\nu = 5$

From Fig.13 and Fig.15, it can also be inferred that circulations are very strong at $\phi = \pi/2, 3\pi/2$ where the voltage peaks are found. The magnitude of the voltage or the electric field determines the magnitude of nn_E and $n\theta_E$, because of very high $n\theta_E$ at the voltage peaks $\phi = \pi/2, 3\pi/2$ as shown in Fig. 18 and Fig.19, the circulations are significant compared to the lower portion of the voltage peak especially at $\phi = 0, \pi$ where the dominant force acting on the interface is the surface tension force which is trying to bring the drop shape to the initial spherical shape.

Streamlines (Fig.12 and Fig.14) cut through the surface in the entire cycle indicating that there are surface velocities which keeps the interface in motion for the entire cycle.

5.4. Effect of Ca_E on mixing for Ca_E = 40 and 80 at a constant dimensionless frequency = 5

It has been shown that the maximum increase in the rate of heat transfer with uniform electric field is 67% compared to heat transfer to a purely translating drop without application of electric field (Oliver et al., 1985). It is hypothesized that alternating electric field will cause a time varying flow field and continuous drop oscillations that will lead to a particle path deviant from the normal circular path at steady state.

In Figures. 20-22, trajectory of three particles are obtained for a droplet with zero oscillation or for a droplet subjected to a steady electric field. It was observed that both the particles tracked, repeat the same circular path irrespective of the time it was tracked. The flow field inside a droplet for $Ca_E = 80$, when subjected to a steady electric field does not change with time as shown in fig.6, hence the particle tend to move in the same path.

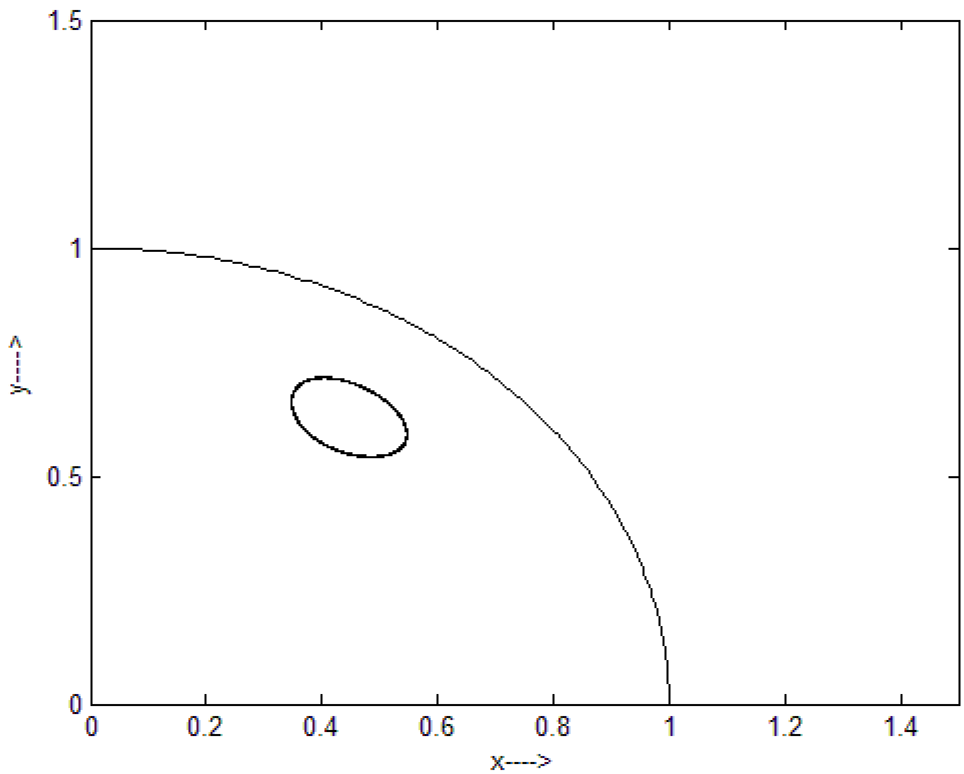

Figure 20. Trajectory of 2 particles after a time t = 320 inside a droplet with no deformation

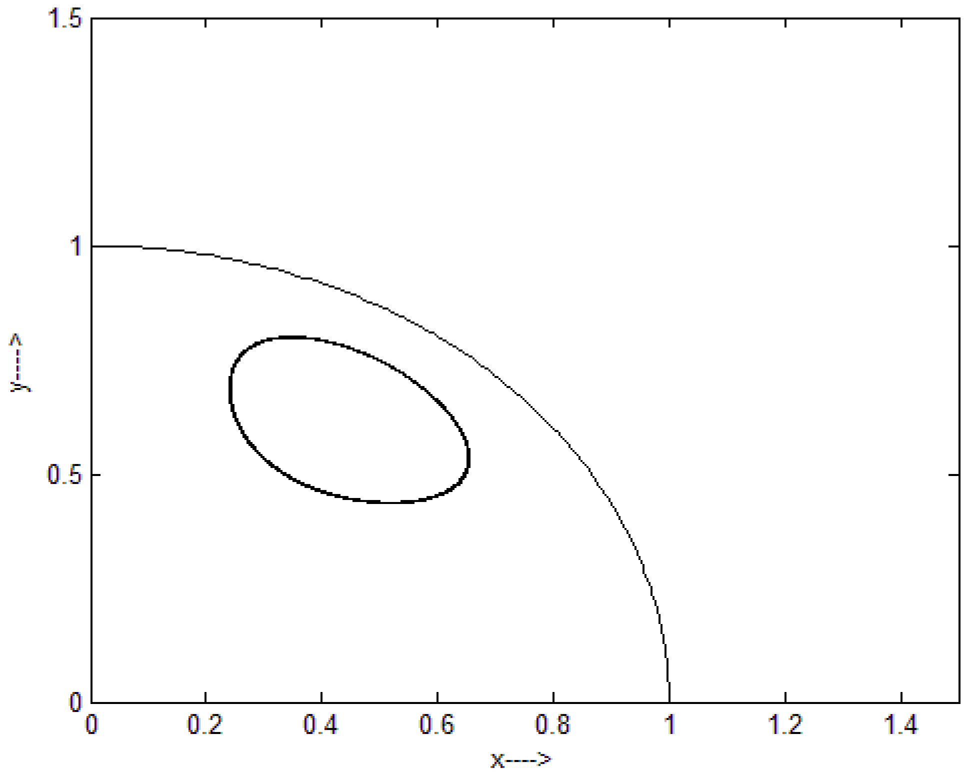

Figure 21. Trajectory of 2 particles after a time t = 320 inside a droplet with no deformation

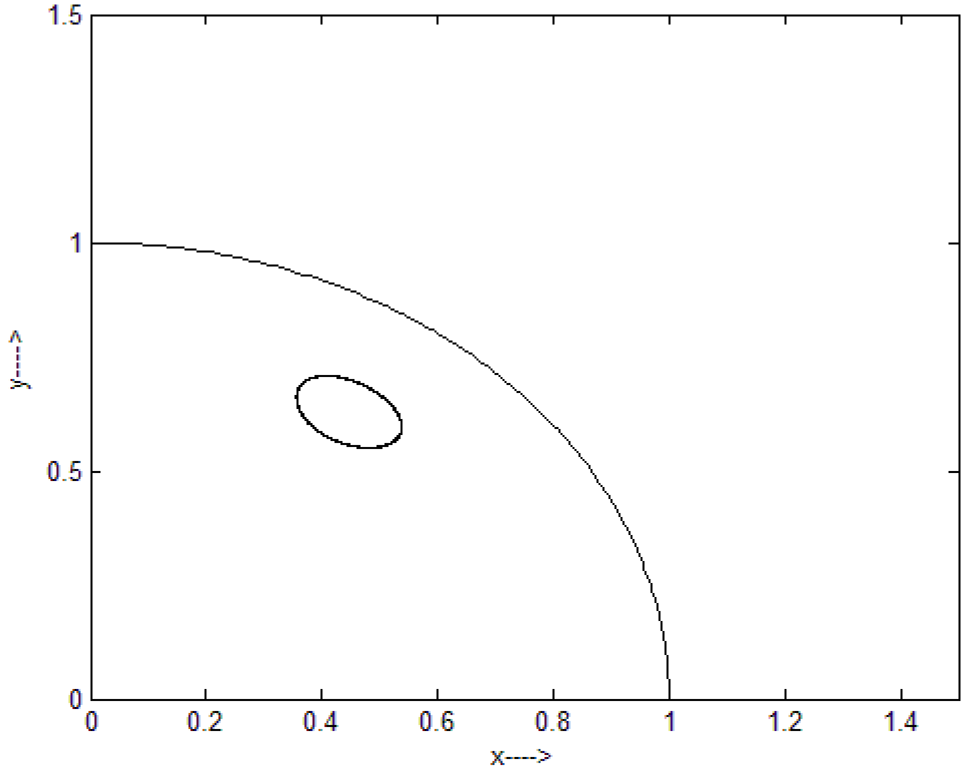

Figure 22. Trajectory of particle 3 after a time t = 320 inside a droplet with no deformation

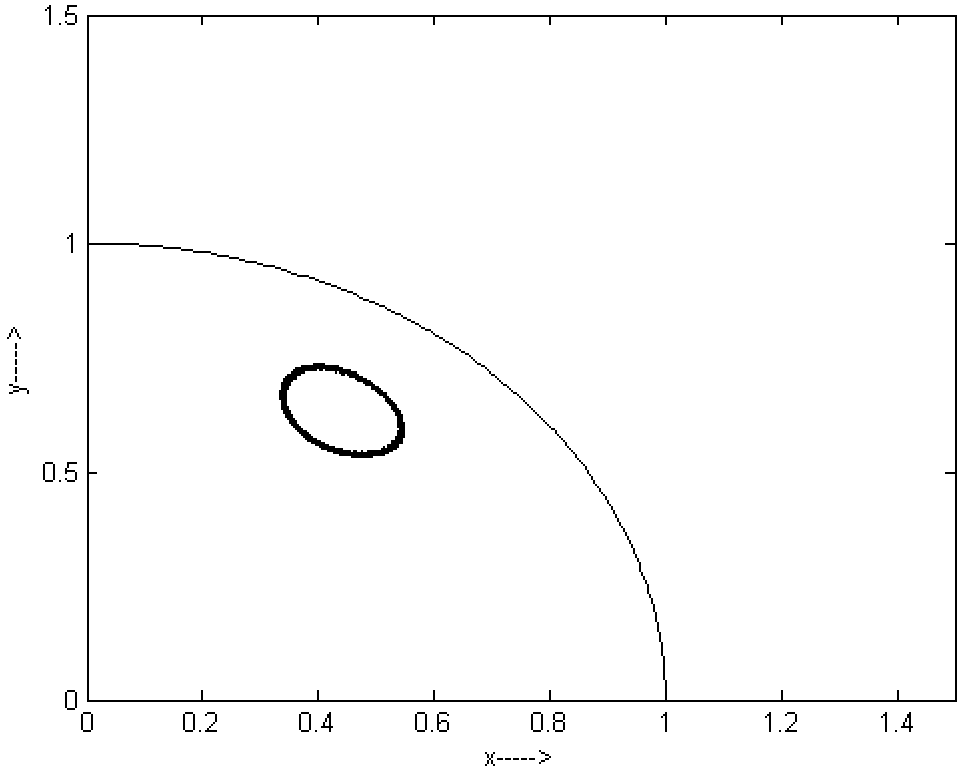

Figure 23. Trajectory of particle 1 inside a droplet for $Ca_E = 40$, $\nu = 5$ after time t = 320

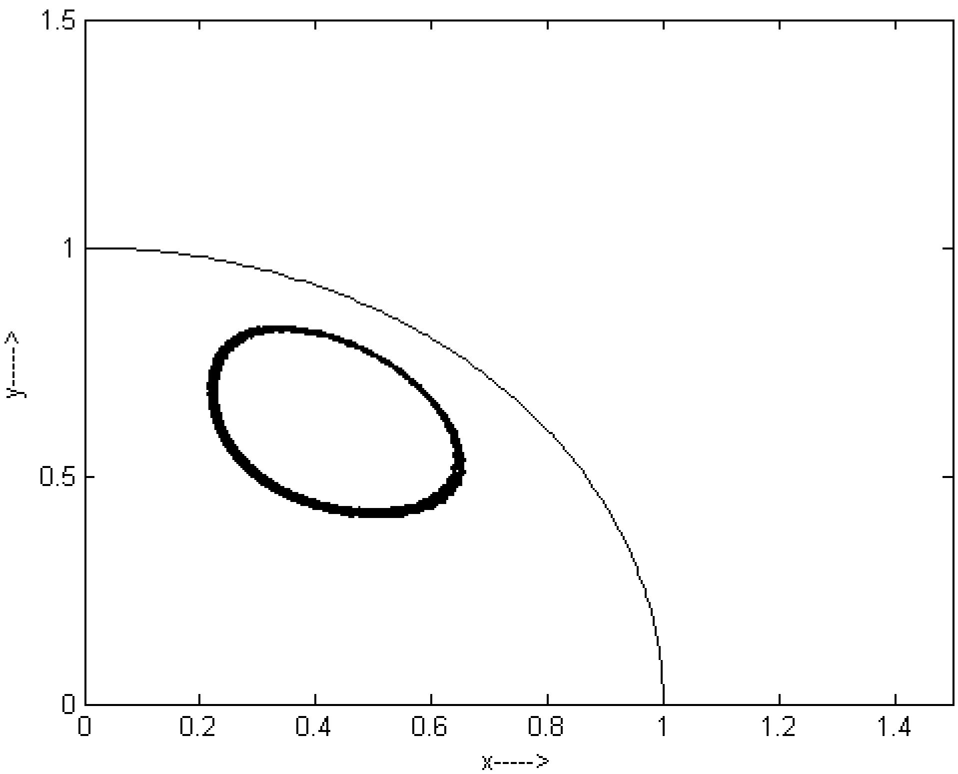

Figure 24. Trajectory of particle 2 inside a droplet for $Ca_E = 40$, $\nu = 5$ after time t = 320

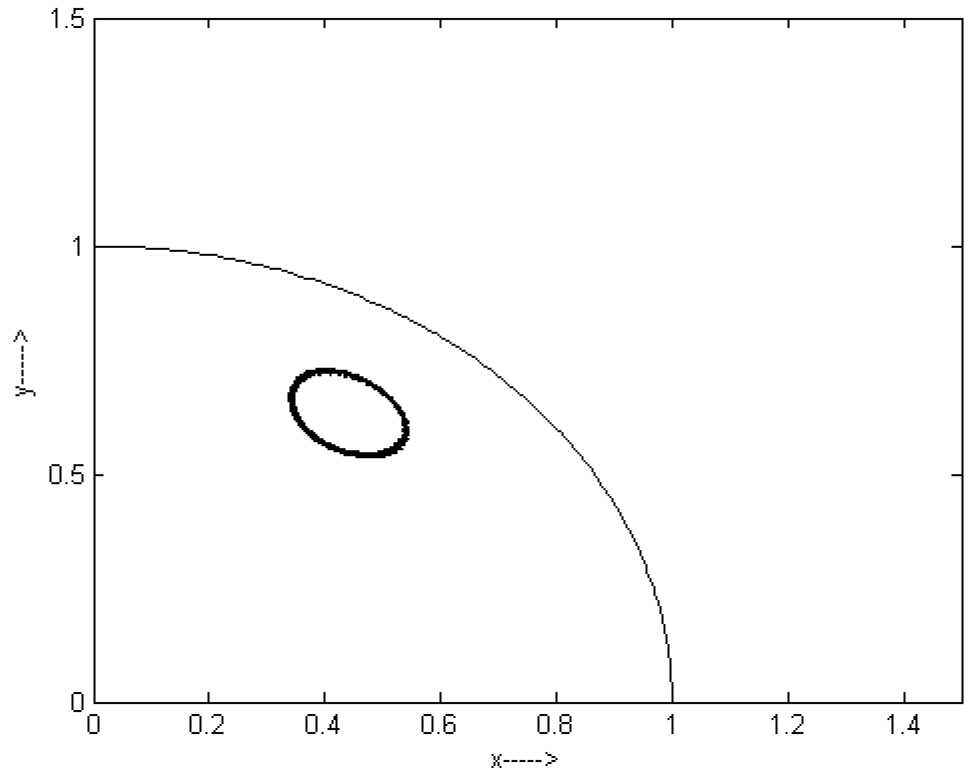

Figure 25. Trajectory of particle 3 inside a droplet for $Ca_E = 40$, $\nu = 5$ after time t = 320

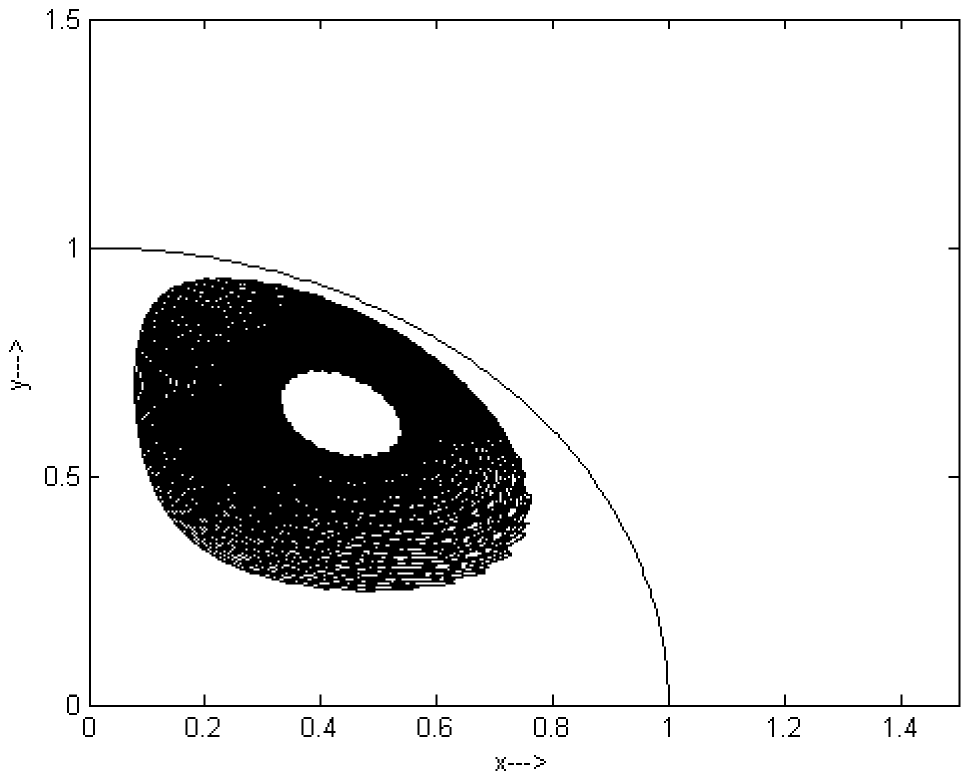

Figure 26. Trajectory of particle 1 inside a droplet for $Ca_E = 80$, $\nu = 5$ after a time t = 320

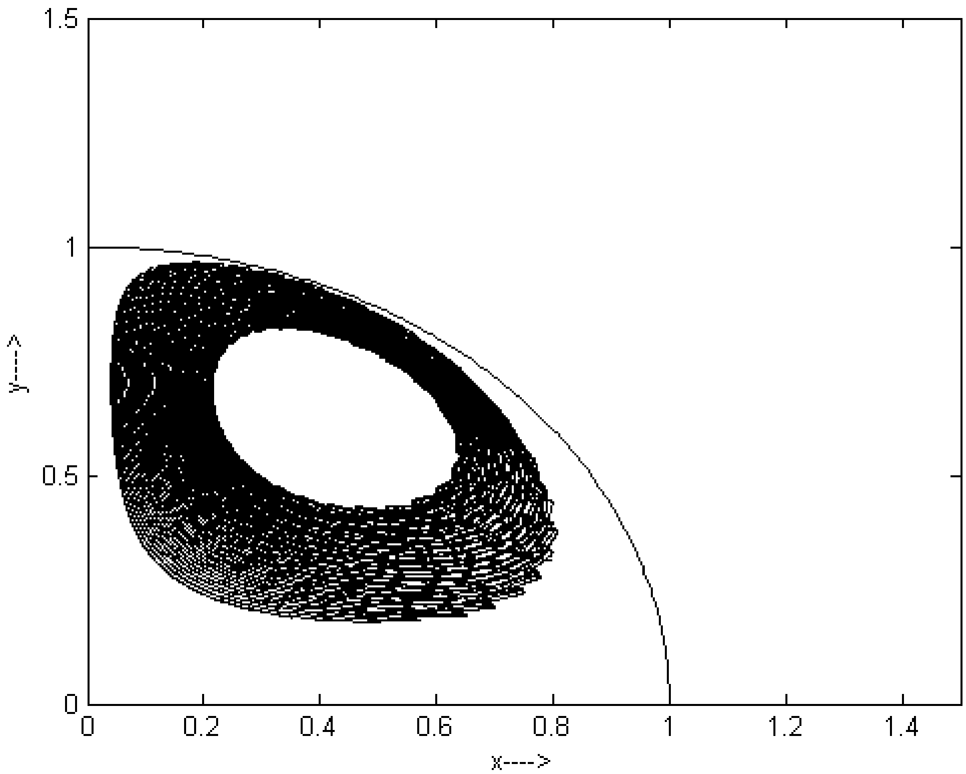

Figure 27. Trajectory of particle 2 inside a droplet for $Ca_E = 80$, $\nu = 5$ after a time t = 320

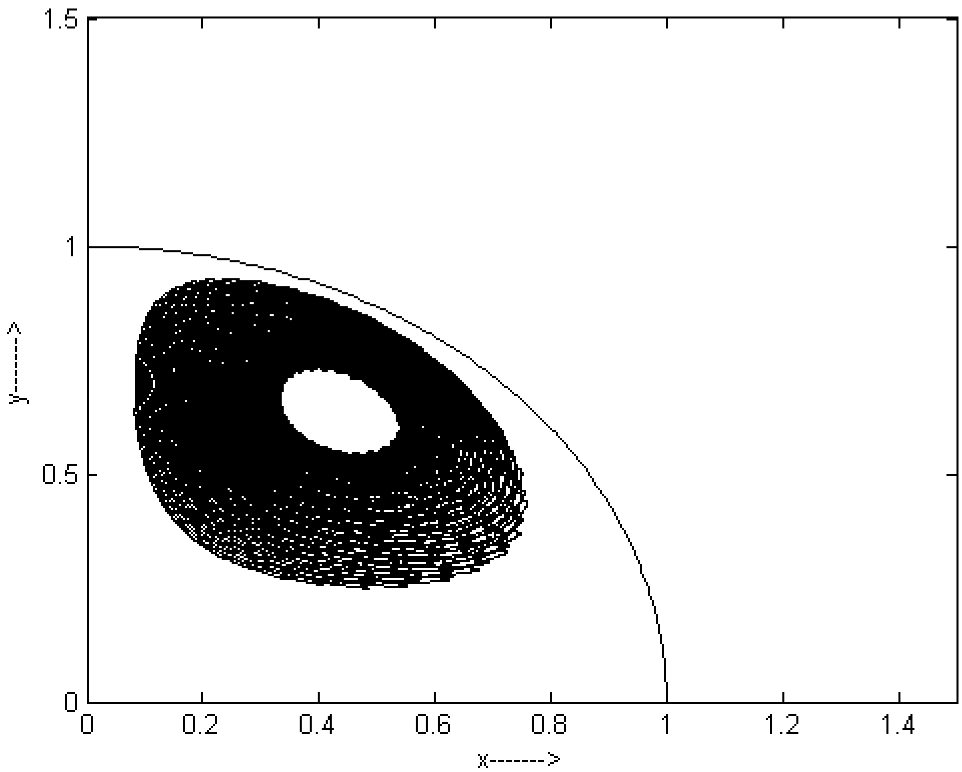

Figure 28. Trajectory of particle 3 inside a droplet for $Ca_E = 80$, $\nu = 5$ after a time t = 320

.

In Figures 23-25 and 26-28, trajectory of three particle inside a droplet are plotted for Ca_E = 40 and 80 respectively. Particle trajectory for Ca_E = 40 and Ca_E = 80 inside a droplet forms a band compared to the particle trajectory inside a droplet with no deformation (Fig. 22), It can be qualitatively concluded from the plots that there is a significant amount of mixing inside a droplet which is oscillating compared to a droplet with zero oscillation.

It is also observed from Figs. 23-25 and Figs. 26-28 that the band width of the particle trajectory for Ca_E = 80 is much greater than Ca_E = 40, which signifies that the extent of mixing taking place inside the droplet is much higher for Ca_E = 80 than 40. Electric capillary number (

Ca_E) gives the measure of electrical force over the surface tension force, by increasing Ca_E the deformation of the drop increases, so is the oscillation allowing the particle to cover a larger area.

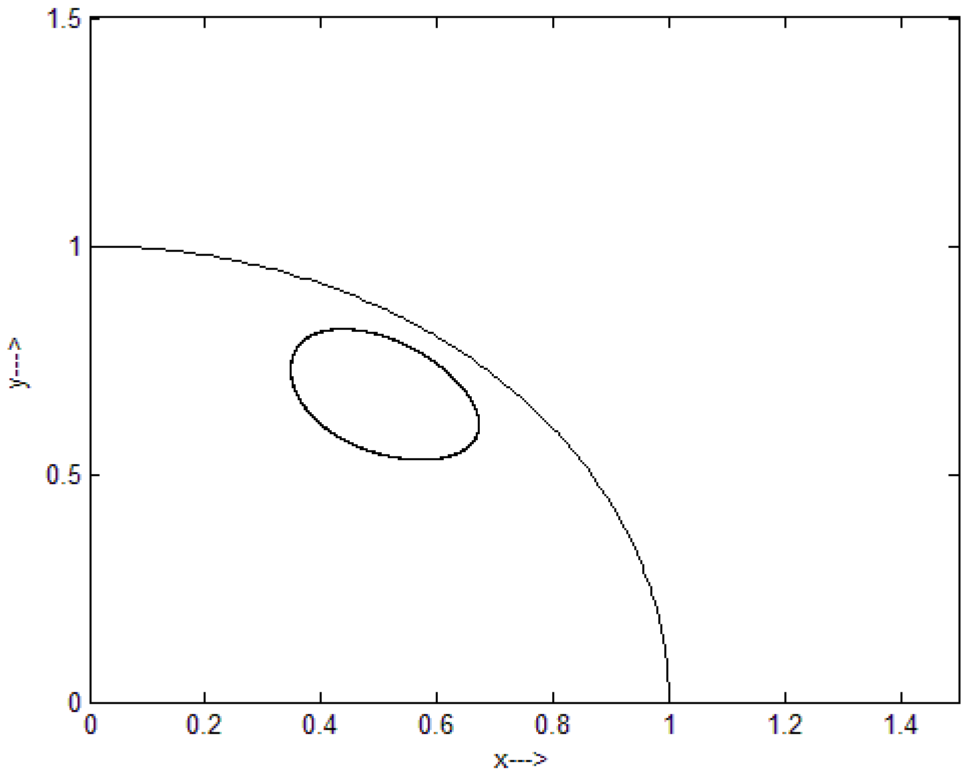

Figure 29. Trajectory of particle 1 inside a droplet for $Ca_E = 80$, $\nu = 50$ after a time t = 320

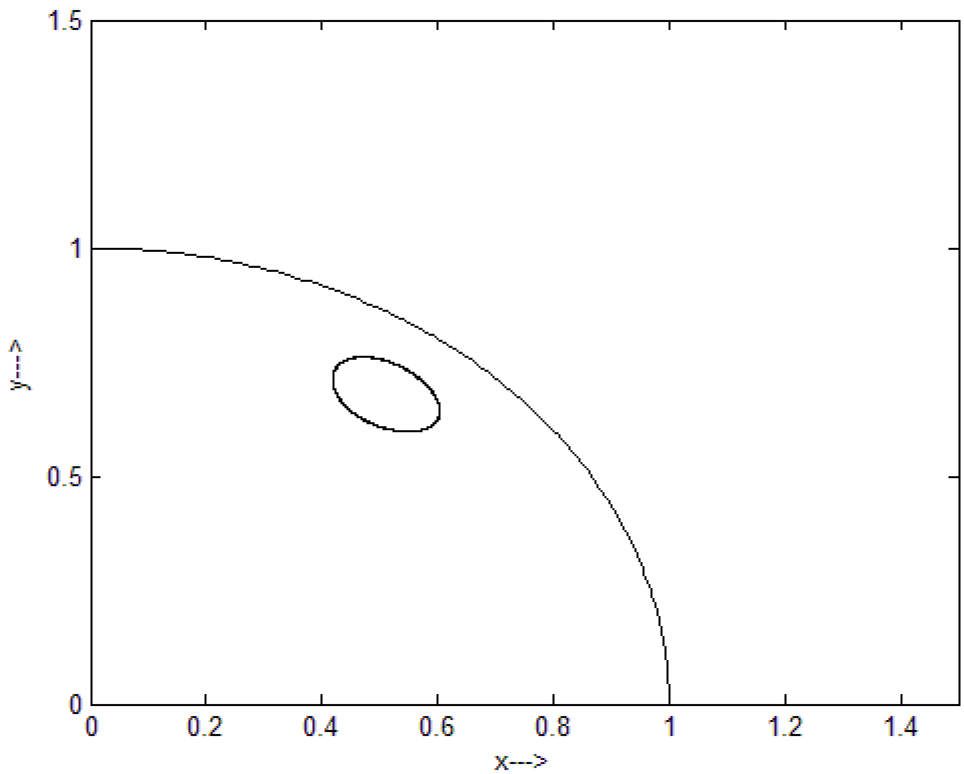

Figure 30. Trajectory of particle 2 inside a droplet for $Ca_E = 80$, $\nu = 50$ after a time t = 320

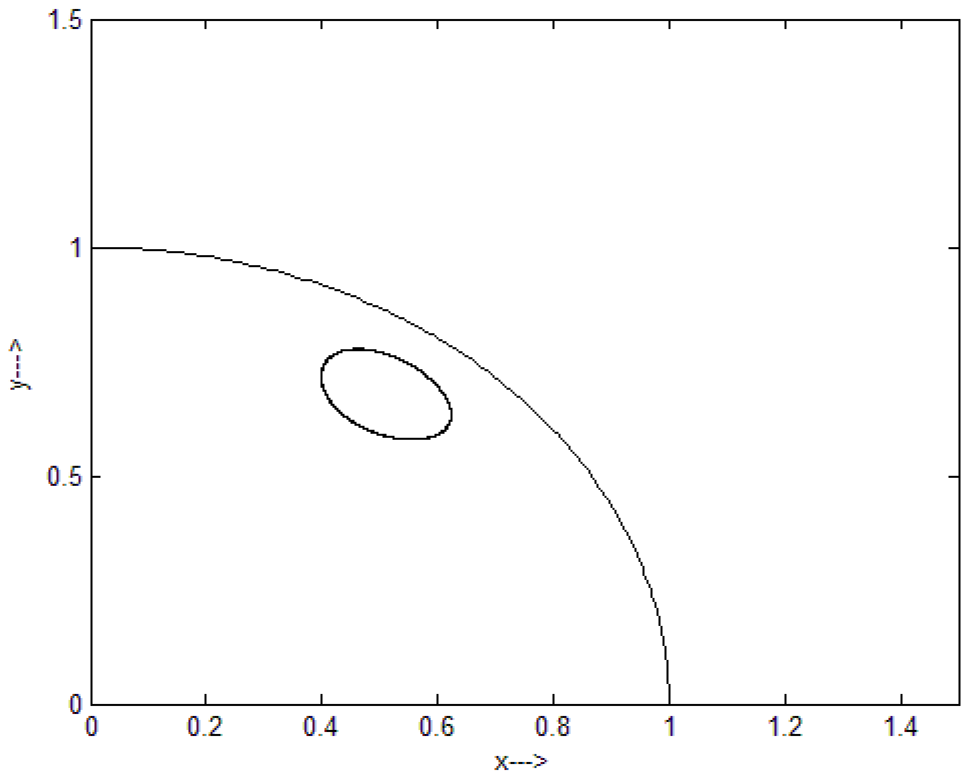

Figure 31. Trajectory of particle 3 inside a droplet for $Ca_E = 80$, $\nu = 50$ after a time t = 320

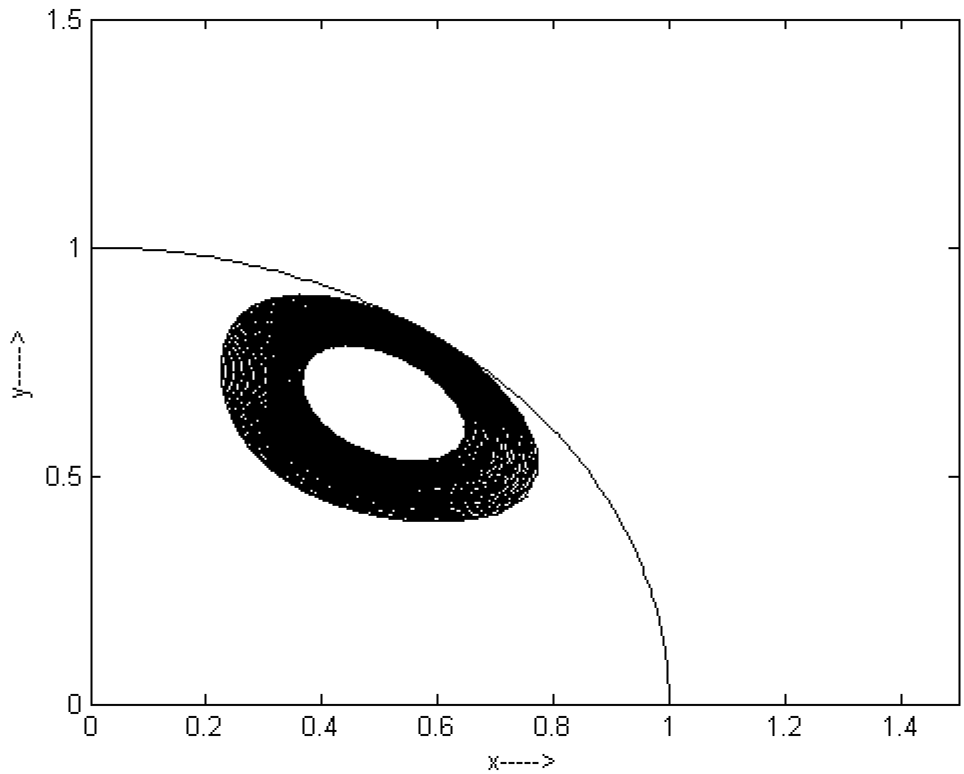

Figure 32. Trajectory of particle 1 inside a droplet for $Ca_E = 80$, $\nu = 15$ after a time t = 320

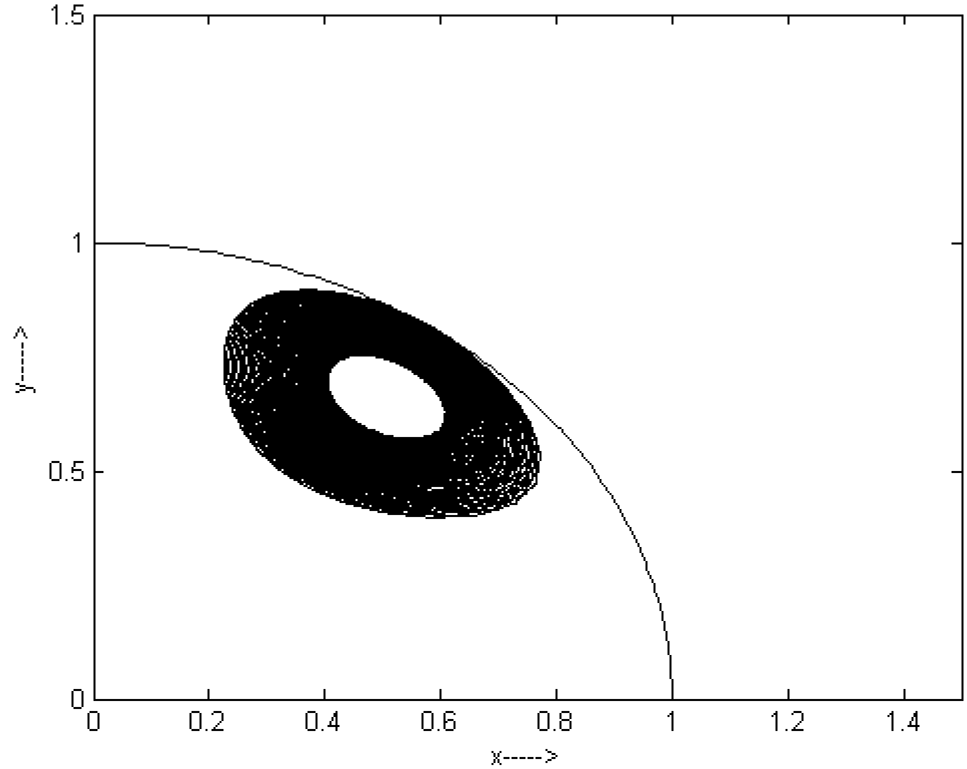

Figure 33 Trajectory of particle 2 inside a droplet for $Ca_E = 80$, $\nu = 15$ after a time t = 320

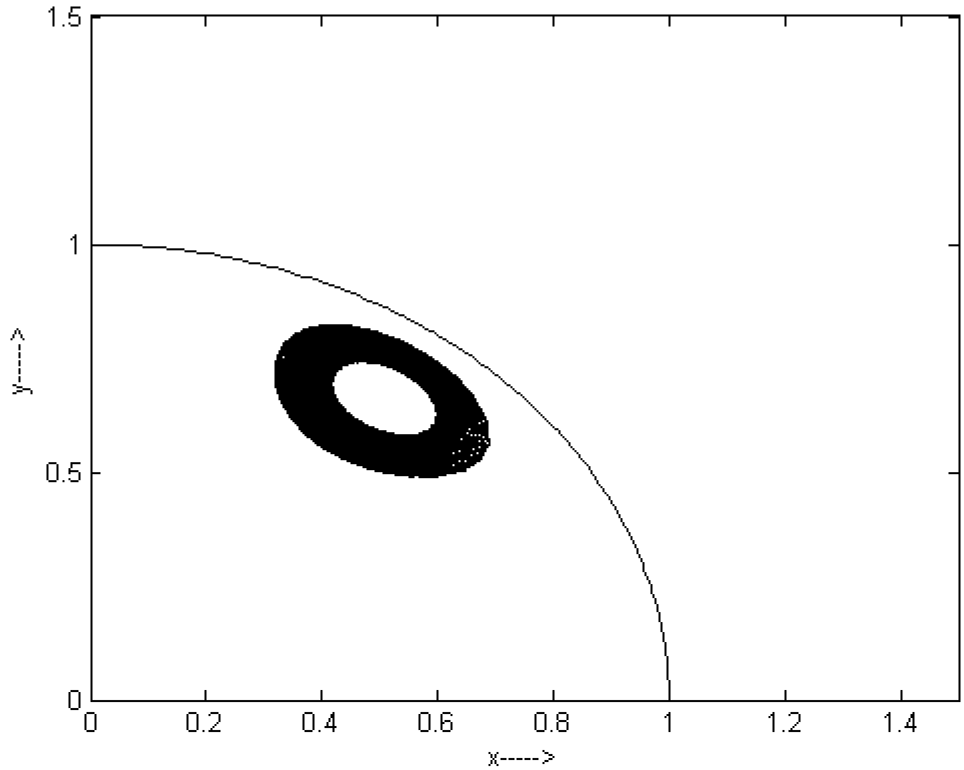

Figure 34. Trajectory of particle 3 inside a droplet for $Ca_E = 80$, $\nu = 15$ after a time t = 320

5.5. Effect of frequency on mixing at a constant Ca_E = 80

In Figures 29-31, 31-33 and 33-35, the particle trajectories inside a droplet are plotted for ν = 50, 15 and 5 at a constant Ca_E = 80. It is observed that for ν = 50, the particle retraces the same circular path, but for ν = 15 a band is formed, as the frequency decreases the band width increases implying greater mixing.

When the frequency is high as in the case of ν = 50, the voltage shoots up to its maximum value within a short interval of time restricting the droplet to deform and retain the initial spherical shape. As the frequency decreases, the voltage gradually increases with time allowing the droplet to deform well enough to increase the oscillation. The increase in deformation thereby oscillation leads to better mixing inside the droplet at low frequencies.

CHAPTER 6

CONCLUSIONS AND RECOMMENDATIONS FOR FUTURE WORK

6.1 Conclusions:

The mixing inside the droplet subjected to an alternating electric field has been studied. An unsteady axisymmetric flow by varying the electric capillary number (Ca_E) and frequency with constant thermo physical properties was considered. The flow field was solved with a vorticity-stream function formulation and coupled with the deformations caused due to alternating nature of the electric field, by the VOF advection equation. The effects of Ca_E and frequency on mixing were studied. The results for the flow field, stress field, voltage field and mixing (particle trajectory) were obtained. From the results obtained the following conclusion can be drawn:

1. The time period of repetition of flow field is half that of the voltage field, indicating that the Electric stress field is not a function of the sign of the voltage. The stress profile is the same for both positive and the negative voltage half cycle.

2. Two circulations are found at the voltage peaks, $\phi = \pi/2, 3\pi/2$ where the electric stresses are dominant over surface tension force compared to the lower portion of the voltage peak especially at $\phi = 0, \pi$ where a single circulation is found where the dominant force acting on the interface is the surface tension force which is trying to change the drop shape to initial spherical shape.

3. The particle tracked inside a droplet with no deformation moves in a circle or repeats the same path irrespective of the time it is tracked, while the trajectory of the particle tracked inside a droplet with deformation for Ca_E = 40, 80, forms a band which shows there is a mixing.

4. The trajectory of the particle tracked for Ca_E = 80 forms a bigger band than Ca_E = 40, which shows the mixing inside the droplet is significantly higher for Ca_E = 80 than 40.

5. The extent of mixing is inversely proportional to the frequency, because as the frequency was decreased the particle tracked inside the droplet covered a larger area compared to a particle tracked at a higher frequency.

6.2 Scope for future work:

1. The effect of fluid mixing inside a droplet subjected to an alternating electric field on heat and mass transfer can be studied solving the energy and species conservation equations with the Navier-Stokes equations.

2. The mixing properties inside a droplet translating in a dielectric medium coupled with the droplet deformations due to an alternating electric field can be studied.

3. The mixing properties inside a droplet subjected to alternating electric field for very high electric capillary numbers > 100 can be studied.

REFERENCES:

1. Abdelaal, M.R. and Jog, M.A. "*Steady and time-periodic electric field-driven enhancement of heat or mass transfer to a drop: Internal problem* ," 2012a. Int. J. Heat and Mass transfer, Vol. 55, pp. 251-259.

2. Abdelaal, M.R. and Jog, M.A. "*Heat/mass transfer from a drop translating in steady and time periodic electric fields: External problem,*" 2012b. Int. J. Heat and Mass transfer, Vol. 55, pp. 2315 - 2327.

3. Allan, R.S. and Mason, S.G. "*Particle behavior in shear and electric fields,*" 1961. Proc. Roy. Soc., Vol. 267, pp. 45 - 61.

4. Aulisa, E., Manservisi, S., Scardovelli, R. and Zaleski, S. "*Interface reconstruction with least squares fit and split advection in three-dimensional Cartesian geometry,*" 2007. J. of Computational Physics, Vol. 225, pp. 2301 - 2319.

5. Brackbill, J.U., Kothe, D.B. and Zemach, C. "*A continuum method for modeling surface tension,*" 1992. J of Computational Physics, Vol. 100, pp. 335 - 354.

6. Bryden, M.D. and Brenner, H. "*Mass transfer enhancement via chaotic laminar flow within a droplet,*" 1999. Int. J. Fluid Mech., Vol. 379, pp. 319 - 331.

7. Chester, T., Konski, O. and Thacher, H. "*The distortion of aerosol droplets by an electric field,*" 1953. J. of Phys. Chem., Vol. 57, pp. 955 - 958.

8. Christov, C.I. and Homsy, G.M. "*Enhancement of transport from drops by steady and modulated electric fields,*" 2009. Phys. Fluids, Vol. 21, p. 083102 .

9. Geoffrey, T. "*The circulation produced in a drop by an electric field,*" 1966 Proc. Roy. Soc., Vol. 291, pp. 159 - 166.

10. Hader, M.A and Jog, M.A. "*Effect of drop deformation on heat transfer to a drop suspended in an electric field,*" 1998. Journal of Heat Transfer, Vol. 120, pp. 682 - 689.

11. Harlow, F., Welch JE. "*Numerical calculation of time-dependent viscous incompressible flow of fluid with a free surface,*" 1965. Phys. Fluids, Vol. 8, pp. 2182 - 2189.

12. Hirt, C.W. and Nichols, B.D. "*VOF method for the dynamics of free boundaries,*" 1981, J. of Computational physics. Vol. 39, pp. 201 – 225.

13. Jog, M.A. and Hader, M.A. "*Transient heat transfer to a spheroidal liquid drop suspended in an electric field,*" 1997. Int. J. Heat and fluid flow, Vol. 18, pp. 411 - 418.

14. Meizhong, D., Perot, J.B. and Scmidt, D.P. "*Heat transfer within deforming droplets,*" 2002. Proc. Of ASME.

15. Noh, W.F, Woodward. P. "*SLIC (Simple line Interface Calculation).*" 1976. Proceedings of Fifth International Conference on Numerical methods in Fluid Dynamics, Enschede. Lecture Notes in Physics, Vol.59, pp. 330 - 340.

16. Oliver, D.L.R, Carlson, T.E and Chung, J.N. "*Transient heat transfer to a fluid sphere suspended in an electric field,*" 1985, Int. J. Heat Mass Transfer, Vol. 28, pp.1005 - 1009.

17. Osher, S. and Sethian, J.A. "*Fronts propagating with curvature dependent speed: Algorithms based on Hamilton Jacobi formulations,*" 2000. J. of computational physics. Vol.79, pp. 12 - 49.

18. Subramanian, R., Jog, M.A. "*Enhancement of heat transfer by an electric field for a drop translating at intermediate Reynolds number*". 2005. Journal of heat transfer. Vol. 127, pp. 1087 - 1095.

19. Sussman, M. and Puckett, E.G. "*A coupled level set volume of fluid method for computing 3D and axisymmetric incompressible two-phase flows,*" 2000. J. of computational physics. Vol. 162, pp. 301 - 337

20. Torza, S., Cox, R.G. and Mason, S.G. "*Electrohydrodynamic deformation and burst of liquid drops,*" 1971. Proc. Roy. Soc., Vol. 269, pp. 295 - 319

21. Ward, T. and Homsy, G.M. "*Electrohydrodynamically driven chaotic mixing in a translating drop,*" 2001. Phys. Fluids, Vol. 13, pp. 3521 - 3525.

22. Ward, T. and Homsy, G.M. "*Electrohydrodynamically driven chaotic mixing in a translating drop II. Experiment,*" 2003. Phys. Fluids, Vol.15, pp. 2987 - 2994.